RSC Chemical Biology

ROYAL SOCIETY OF CHEMISTRY

REVIEW

View Article Online
View Journal | View Issue

Cite this: *RSC Chem. Biol.*, 2025, **6**, 1048

Metal-mediated peptide processing. How copper and iron catalyze diverse peptide modifications such as amidation and crosslinking

Ninian J. Blackburn

Peptide processing is an important post-translational function that converts newly synthesized pro-peptides into their biologically active mature forms. In this review we discuss two such processes, peptide amidation and ribosomally synthesized post-translationally modified peptide (RiPP) synthesis. The first step in peptide amidation is catalyzed by copper, utilizing a single enzyme peptidylglycine monooxygenase (PHM), while RiPP chemistry can utilize Fe-containing radical SAM enzymes and in a more recent discovery Cu-containing burpitide cyclases. For PHM we describe the canonical mechanism built on three decades of structural, spectroscopic and computational work that posits mononuclear reactivity coupled to long range electron transfer. We discuss this alongside new experimental evidence that suggests instead an open-to-closed conformationally gated mechanism where a binuclear copper entity is the reactive species. Next we describe new insights into RiPP chemistry of thioether formation formed *via* cysteine to peptidyl-C crosslinking in the radical SAM enzymes PapB and Tte1186. Here Se edge XAS has documented selenocysteine to Fe binding at an auxiliary FeS cluster as an important step in S/Se to peptidyl-C coupling. Finally we examine analogous radical-induced peptide crosslinking in a new class of peptide cyclases termed burpitide cyclases (BpCs) some of which exhibit a striking similarity to PHM, yet show catalytic chemistry leading to a different product profile. These comparisons emphasize how nature leverages very specific properties of metal ions, and their ability to underpin catalysis *via* radical processes to bring about a variety of important biochemical and biological outcomes.

Received 8th April 2025,
Accepted 4th June 2025

DOI: 10.1039/d5cb00085h

rsc.li/rsc-chembio

Introduction

Peptide processing is an important post-translational function that converts newly synthesized pro-peptides into their biologically active mature forms.[1–4] Most bioactive peptides are synthesized in their pro-peptide form where the N-terminal sequence is used for trafficking or for recognition of cognate enzyme partners. Important peptide processing pathways involve C-terminal amidation, and ribosomally encoded post-translational peptide synthesis (RiPP) which generate active neuropeptide hormones and cross-linked bioactive molecules respectively.

Amidated peptides are important regulators of cellular function *via* interactions with GPCRs at the cell membrane to initiate a molecular cascade leading to production of essential hormones.[3,5,6] A contemporary example is the action of glucogen-like peptide 1 (GLP1) on pancreatic beta cells to regulate the production of insulin leading to the current use

Department of Chemical Physiology and Biochemistry, Oregon Health & Sciences University, Portland, OR 97239, USA. E-mail: blackbni@ohsu.edu

Ninian J. Blackburn

Dr Ninian Blackburn received his doctorate from the University of Dundee in 1974. After post-doctoral studies in Oregon and Leeds he joined the faculty of the University of Manchester Institute of Science and Technology as a lecturer in Chemistry in 1979. In 1987 he moved to the USA where he was appointed Professor first at the Oregon Graduate Institute and later at Oregon Health and Sciences University in Portland where he remains on the faculty in the Department of Chemical Physiology and Biochemistry. He has served on numerous National Institutes of Health (NIH) study sections and review panels for the Stanford Lightsources both SSRL and the LCLS. He is currently Chair of the Structural Molecular Biology Advisory Committee at SSRL. He has published over 150 peer review papers and has received continuous funding from NIH since 1989.

of GLP1-related drugs in the treatment of T2 diabetes.[6] While native GLP1 peptides are susceptible to proteolysis, minor changes in sequence can generate synthetic analogues with improved pharmacokinetics – the semaglutide class of drugs that include Ozempic and Wegovy. These drugs have been shown to have remarkable success in the treatment of obesity, so much so that that they are now used as designer drugs for cosmetic weight loss. However, the GLP1s do have side effects, most notably an increased risk of medullary thyroid cancer. Understanding the biochemical mechanisms that underpin native synthesis and degradation of amidated peptides is important because other neuropeptides can have opposite physiological effects which complicate therapeutic outcomes. For example, neuropeptide Y expressed predominately in GABAergic neurons of the hypothalmus and hippocampus acts post-synaptically on GPCR Y receptors to regulate food intake, fat storage, and bring about reduction in pain perception, anxiety, and alcohol intake. Its function appears opposite to GLP1s in that high levels lead to obesity *via* a process that includes stimulation of gluconeogenesis, down-regulation of leptin and/or its receptor and induction of insulin resistance.[5] These examples illustrate the important and often antagonistic roles of amidated peptides in human health, and given the broad scope of these molecules in hormonal regulation, they remain good targets for drug interventions provided that their complex interactions can be fully understood. Other examples of amidated peptides include thyroid stimulating hormone (TSH), oxytocin (OT), calcitonin (CT), growth hormone releasing factor (GHRF), and more.

Peptide processing *via* other pathways is also known to be a major source of new lead compounds for antibacterial, antiviral and anticancer therapeutics. Traditionally non-ribosomal peptide synthesis (NRPS) has generated many of the common antibiotics in use today,[7] but increasing resistance has spurred new discovery science focused on finding alternatives with different modes of action. A class of natural products with enormous potential are the ribosomal synthesized and post-translationally modified peptides or RiPPs which encompass a new class of antibiotics based on lanthipeptides, thiopeptides, sactipeptides, and ranthipeptides many of which carry modifications involving α-, β-, or γ-thioether crosslinks.[2,4] These compounds show activity against Gram positive bacteria, especially *S. aureus* (MRSA) and are therefore of great pharmacological interest. RiPP synthesis involves a precursor peptide and its associated maturase (cyclase) which is often a metalloprotein such as a radical SAM enzyme.[8] The precursor peptide (substrate) is itself comprised of a leader sequence which recognizes the maturase, and a ''core'' peptide which contains the sequence that will be modified. The reactions involve radical mediated crosslinking reactions and are terminated *via* tailoring of the N- and C-termini by proteases to release the mature products.

Peptide processing reactions are often mediated by metals and/or are catalyzed by metalloenzymes. Peptidylglycine alpha-amidating monooxygenase (PAM) is the only enzyme able to catalyze peptide amidation, *via* a mechanism that first converts the glycine-extended pro-peptide to an α-hydroxyglycyl intermediate in a Cu-dependent reaction catalyzed by the PHM (peptidylglycine alpha hydroxylating monooxygenase) domain followed by hydrolysis of the carbinolamide to form the peptide amide and glyoxalate in a Zn/Ca-dependent process catalyzed by the PAL (peptidylglycine alpha amidating lyase) domain (Fig. 1(a)).[3,9] AhyBURP is a member of an emerging class of copper-dependent peptide cyclases (burpitide cyclases or BpCs) within the broader class of RiPP enzymes which install tyrosine or tryptophan crosslinks.[1,10–12] BpCs are unusual since often a single protein contains both the core peptide and its maturase, such that the ribosomally encoded precursor is autocatalytic.

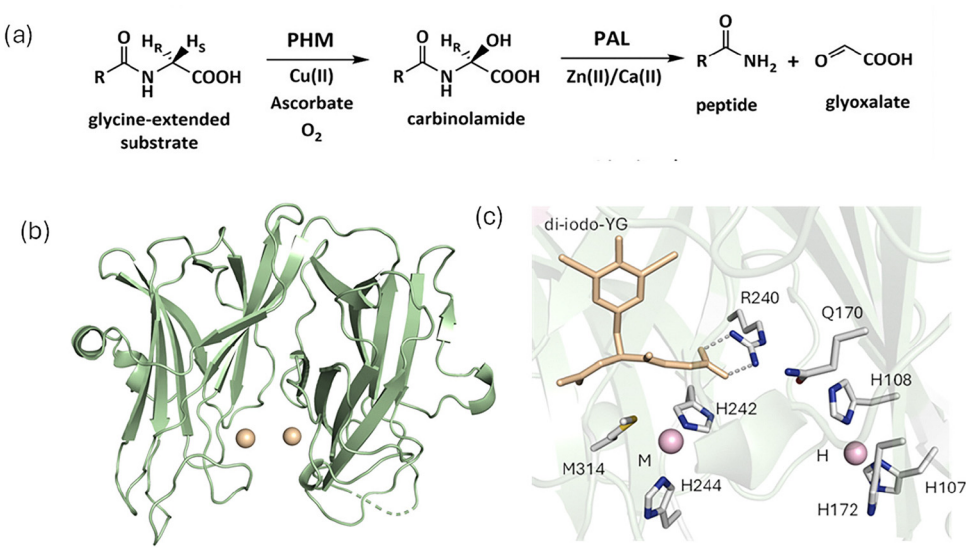

Fig. 1 (a) Reaction catalyzed by peptidylglycine alpha-amidating monooxygenase (PHM and PAL). (b) Subdomains of the PHM structure showing the Cu atoms in gold separated by 11 A. The M-subdomain is on the left, the H subdomain is on the right. (c) Active site of the substrate-bound enzyme showing the positions of the Cu ligands and substratedi-iodo YG substrate in the pocket. From pdb file 1OPM.

Although unrelated in sequence or protein fold, the AhyBURP active site bears a remarkable resemblance to PHM in metal site coordination and separation, the presence of an unusual disulfide staple at each of the two copper sites, and the proposal for a parallel reaction mechanism.[10] Both AhyBURP and PHM generate a substrate radical *via* oxygen chemistry at their homologous Cu(I) His_2Met copper centers but thereafter the reactions diverge. In PHM, the product is an α-hydroxyglycine modified C-terminus which is further processed to an amide, while in BURP radical coupling generates two sequential cross-linked products. As mentioned above other RiPP cyclases utilize radical SAM enzymes where the *S*-adenosylmethionine cofactor and its associated Fe/S cluster initiate radical chemistry which is further directed into peptidyl crosslinks *via* downstream auxiliary Fe/S cluster-peptide interactions.[8]

Copper monooxygenases related to PHM also play important roles in neurotransmitter biosynthesis. Dopamine β-monooxygenase (DBM)[13–15] and its insect homologue tyramine β-monooxygenase (TBM)[16] catalyze the biosynthesis of norepinephrine and octopamine respectively. Other non-related monooxygenases include particulate methane monooxygenase (pMMO) and lytic polysaccharide monooxygenase (LPMO), both important in climate mitigation.[17–21] pMMO converts the greenhouse gas methane to methanol while LPMOs catalyze the oxidation of polysaccharides at C1 and/or C4, an important stimulus for biomass degradation. Understanding their underlying reaction mechanisms is therefore important to the health of the planet and its inhabitants.

Peptide amidation

Structure, spectroscopy and canonical reaction mechanism

Structures of WT PHM in oxidized, reduced and substrate-bound forms. The first structure of a PAM domain was that of the catalytic core of the monooxygenase domain (PHMcc, residues 42–356) published in 1997 by Amzel and coworkers.[22] The enzyme was composed of two domains each of which harbored a copper atom with the polypeptide arranged predominately as anti-parallel beta-sheets. These domains were connected by a short loop made up of residues 198–201 (Fig. 1) arranged such that they could rotate relative to each other about a hinge at Ile 201, but (*vide infra*) appeared to be rigid in the crystalline state. Each domain bound a single Cu atom, with the N-terminal domain Cu (termed CuH) coordinated by His 107, His 108, and His 172, and the C-terminal domain Cu (termed CuM) coordinated by His 242, His 244 and Met 314. The Cu atoms faced each other across a solvent-filled cleft between the subdomains with a Cu–Cu separation of ∼11 Å. The dipeptidyl substrate di-iodotyrosylglycine was found to bind *via* its carboxy terminus to Arg 240 where it formed a simple salt bridge to the positively charged guanidinium group, and *via* two secondary interactions with Tyr318 and Asn316. The alpha-C destined for hydroxylation was positioned with its pro-S H atom pointing towards the CuM center. In a subsequent paper[23] they compared the structures of the ascorbate-reduced enzyme and the substrate-bound oxidized enzyme from which they determined (i) enzyme was active in the crystalline state (ii) that little change in copper coordination occurred as a result of redox and (iii) that an electron transfer pathway from CuH to CuM could be traced from H108 *via* Gnl170 a water molecule and thence to the carboxylate O of the substrate. As indicated above an important element of these early observations was the near constancy of the Cu–Cu distance leading to the conclusion that interdomain movement was not a feature of the mechanism. In a third and now classical paper[24] they described an oxygen adduct bound at the CuM center in a structure of PHM with the slow substrate tyrosyl-D-threonine, but here the O–O bond pointed away from the substrate C-alpha in what appeared to be a non-productive or pre-catalytic conformation. Nevertheless, these crystallographic studies were used to propose a plausible mechanism for enzyme catalysis where O_2 first bound at the CuM site to generate a cupric superoxo capable of abstracting the pro-S hydrogen atom from the peptide C-alpha to form Cu(II)-peroxo and a substrate radical, which was further converted to products by radical rebound and long-range electron transfer mediated by the H108-Gln170-water-substrate pathway.

Other structures of PHM derivatives. Structures of a number of small molecule adducts of the oxidized enzyme have been reported. A structure of the hydrogen peroxide adduct shows O_2^{2-} bound exclusively at CuM in a slightly distorted side on configuration[25] while structures of nitrite and azide with oxidized PHM also show selective binding at CuM.[26] For all these adducts the ligands were incorporated into the mother liquor and soaked into the crystals for variable amounts of time. Peroxide at 10 mM bound within 3 minutes while nitrate required 20 h at 300 mM suggesting significant differences in binding affinity. Similarly, adducts with CO were obtained by soaking crystals under 3 atm of CO gas, but here the structures suggest aberrant chemistry in that (i) CO bound to both oxidized Cu(II) and ascorbate-reduced Cu(I) forms, and (ii) the CO ligand was coordinated in a bent configuration with the Cu–C–O angle = 110°.[26] These features of the CO structural chemistry indicate departure from the normal chemistry associated with the interaction of Cu complexes with CO, where CO is expected to bind only to the Cu(I) site with linear geometry and may indicate photoredox chemistry is occurring in the X-ray beam during crystallographic data collection. Other structures of mutant forms of PHM[27] indicate significant interactions between the two copper centers. For example the M314I variant shows that Cu still binds at the M center in a distorted tetrahedral fashion with water replacing the Met314 thioether ligand, but at CuH the H108 ligand appears to have dissociated or is highly disordered, and the H-site shows only partial occupancy. In all of these structures the Cu–Cu separation does not change remaining fixed at ∼11 Å. Diatomic adduct structures are shown in Fig. 2.

EPR and EXAFS spectroscopy. EPR spectra have been recorded and analyzed for both PHM,[28–30] full length PAM[31,32] and the DBM homologue[33] in the resting cupric state. All samples showed close to full occupancy of both sites by Cu(II) with no indication of any magnetic coupling between the unpaired electrons of the individual copper ions, expected if the coppers are closer than ∼4 Å. The EPR parameters are

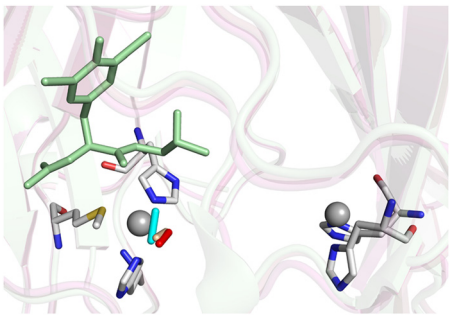

Fig. 2 Structures of the diatomic adducts of PHM bound at the M center. The adducts are shown as colored sticks designated as follows: cyan, peroxide complex of the Cu(II) enzyme(pdb: 4E4Z); red, oxygen complex formed from reduced enzyme + ascorbate (oxidation state undetermined, pdb 1SDW); yellow, CO complex of the reduced enzyme (pdb:3MLJ).

typical of tetragonally distorted non-blue copper centers with N or O coordination and are fully consistent with the ligand sets derived from the crystal structures of the oxidized enzyme. EXAFS spectroscopy has also been used to explore the coordination of the Cu centers in both oxidized and reduced states.[29,31,34] Here significant differences from the crystallography were observed. EXAFS analysis suggested an average Cu(II) coordination of 2.5 His residues and 1.5 O(solvent) with Cu–N/O distances close to 1.95 Å, rationalized by an active site structure represented by CuM-$(His)_2(H_2O)_2$–CuH-$(His)_3(H_2O)$, where each copper adopted a tetragonal structure with 4 equatorial ligands. Although additional longer axial interactions to S(Met314) at the M site or solvent at the H site were anticipated and were supported by ligand field analysis[28] these were completely undetectable by EXAFS. EXAFS studies on the ascorbate-reduced state indicated coordination more similar to the crystallography. The solvent interactions were lost as expected for a Cu(I) site, with the resulting coordination of 2–2.5 His residues and 0.5 S ligands per Cu(I) with Cu–N bond distances of ~1.90 Å and Cu–S(Met314) of ~2.25 Å. Taken together the EXAFS analysis indicated that in solution Met314 moves closer to CuM on reduction, challenging the conclusion from crystallography that no protein conformation changes occurred during catalysis.

Mutant proteins. To further explore the individual roles of each copper, mutant proteins were constructed with variant ligand sets. These included M-site variants M314H[35,36] and H242A,[37] and H-site variants H107A, H108A, H172A, and the H107AH108A double mutant.[38] None of these retained more than ~5% catalytic activity[29,38] but all except H242A and the H-site double mutant H107AH108A bound 2 Cus per protein. H242A and H107AH108A each bound 1 Cu identifying them as M-site and H-site copper deletion mutants respectively.[37] However, despite the low activity of the variants that retained a full complement of copper, like WT their rate of product formation remained completely coupled to oxygen consumption with no evidence for any side reactions where unproductive reduced oxygen species could leak out of the enzyme. Given the large reduction in rates of product formation, this finding is remarkable. For M-site mutants X-ray absorption studies revealed that His314 behaved like Met314 being only detectable by EXAFS in the reduced state while the H242A M-site deletion mutant strongly suggested that the H-site was 2-coordinate in the reduced state with one His ligand dissociated. For H-site mutants solvent appeared to bind in place of histidine to generate 4-or 5-coordinate oxidized H07A and H108A structures, whereas in the reduced proteins any two histidine residues were competent to bind Cu(I), with indications from absorption edge intensities of different degrees of distortion from linearity. Since H107 and H108 are contiguous residues on the same β-strand they are constrained to bind in a *trans* -configuration *via* their Nδ imidazole N atoms which in model systems results in linear geometry[39] a fact previously noted to explain the increased intensity of the 8982 eV edge feature in the XAS of the H172A variant.[40,41] However, the absorption edge intensity for the H107A and H108A variants was comparable to the WT protein, suggesting that they may be unable to adopt the preferred linear structure. These studies together with the fact that most of the loss is in activity was associated with k_{cat} suggests that the H-site requires a unique arrangement of its His ligands for catalytic function.

Kinetics and isotope effects. Kinetic studies of PHM have revealed an equilibrium ordered mechanism in which peptidyl substrate binding precedes that of oxygen.[42–45] Based on the large value of the intrinsic KIE for the chemical step Francisco and coworkers[44] implied a H atom tunneling mechanism although the small isotope effect on k_{cat} suggested that H atom abstraction (HAA) was only partially rate limiting. The isotope studies predicted that the transition state was gated by molecular motions which transiently oriented the reactive species into a productive conformation for H atom transfer, which must occur over short distances due to the large mass of the H atom.[46] This concept was later extended to include two types of motions that generate a pre-organizational state and a reorganizational state[42] where the pre-organizational state referred to the motions of enzyme and substrate required to generate the E–S complex and the reorganizational state referred to the gating motions or vibrations within the protein required for optimizing reactivity. While the identities of these motions are unknown, we may speculate that substrate binding induces some form of conformational transition required for oxygen activation, a phenomenon often referred to as ''substrate triggering''. A requirement for substrate triggering of catalytic activity would be fully consistent with the complete coupling of product formation and oxygen consumption described above.

KIE studies on the H-site variant H172A provided an important and surprising codicil to the mechanistic interpretation of isotope effects.[47] While the mutation lowered rates of substrate binding and electron transfer 400–2000 fold, a much larger effect was observed for the HAA step where the rate was reduced by a factor of 12 000 relative to WT. This implies that H172A has a large influence on the reorganizational energy and/or dynamics required to form the transition state within which HAA chemistry can proceed. While this might involve solvent-induced reorganization of H-bonding pathways or global

conformational effects that perturb the structure of the ES complex, the magnitude of the effect suggests direct structural involvement of this ligand in the transition state. This is a remarkable result for a residue located 8–11 Å from the active site and will be discussed in more detail later in this review.

Computational studies leading to the canonical catalytic mechanism. A number of detailed computational studies have been reported that attempt to correlate transition state structures and energetics with experimentally derived parameters, such as KIE values and estimated rates of individual mechanistic steps. These studies have used a variety of approaches which include QM/MM[48,49] or DFT[50–52] and generally use truncated active site structures based on the crystallographic coordinates as the starting point for geometry optimization, followed by estimation of the energetics of formation and decay of intermediates along the reaction coordinate. The validity of the calculations relies at least in part on the crystallographic description of the CuM–O_2 complex and the fixed Cu–Cu distance of ∼11 Å, and would need to be revisited if further evidence challenged either of these underpinning assumptions. Overall the calculations support a mechanism (Fig. 3) where oxygen binds at CuM to form a CuM-superoxo species which is sufficiently electrophilic to abstract a H atom from the peptide pro-S C-alpha resulting in a substrate radical and a Cu(II)–OOH intermediate. The substrate radical then undergoes rebound with the cupric peroxide *via* attack on the proximal O atom to generate a high energy Cu(II)–O$^{\bullet}$ radical and the hydroxylated product. The final step is long-range electron transfer (ET) from CuH which is energetically more favorable if accompanied by proton transfer (PCET). However, the calculations have shown a tendency to evolve as the level of theory and/or the understanding of parallel chemistry from simpler inorganic models has improved.[53] For example Crespo and coworkers using a QM/MM approach excluded the CuM-superoxo, and Cu(II)-hydroperoxo species as capable of HAA, whereas Cowley and coworkers later reported that Cu(II)-superoxo is indeed competent provided it is formed by displacement of a coordinated water on Cu(I)M. This latter assertion has gained support from a recent study which tested the HAA potential of 4- *versus* 5-coordinate Cu(II)-superoxo complexes which found the 4-coordinate systems to be up to 100 times faster for C–H activation.[54] Additionally the Cowley and Solomon mechanism[52] generated values for isotope effects and electron transfer rates that were in good agreement with those derived experimentally which is necessary (although not sufficient) to determine the mechanism, and provided support for what may be called the canonical mechanism for PHM and DBM catalysis shown in Fig. 3. The authors cited two tenets of this mechanism that were of special interest (i) the Cu(II)-superoxo derives its strong electrophilic character from the large CuM···CuH 11 Å separation since a second electron is excluded from transferring directly to form a Cu(II)M-peroxo species and (ii) the large reorganizational energy of the $Cu(His)_3$ structure of the H site prevents PCET from CuH to CuM until there is sufficient driving force, *i.e.* until an intermediate of sufficiently high redox potential has been generated. There are many aspects of this mechanism that are innovative and unique, but as we shall see, there are many experimental details that are

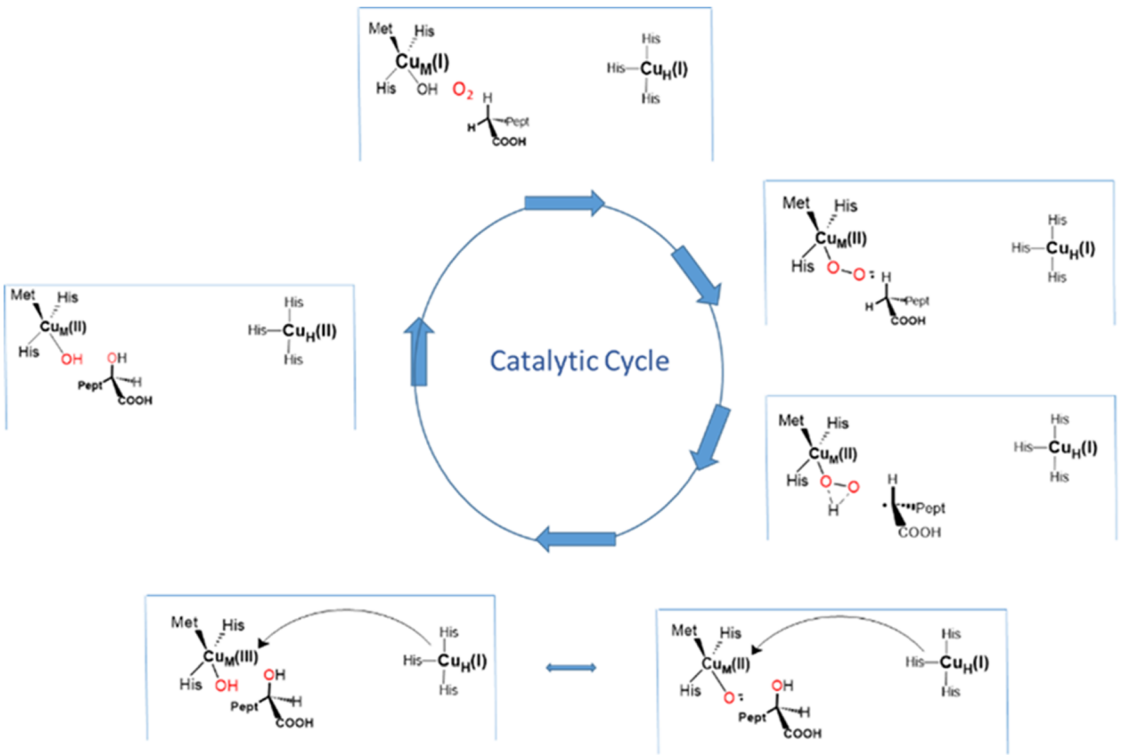

Fig. 3 Canonical mechanism for PHM.

inconsistent, and in general have not been considered in the mechanistic formulation.

Carbon monoxide binding as a probe of oxygen reactivity and substrate triggering

CO as a surrogate for molecular oxygen. Although an oxygen adduct has been isolated in the crystalline state[24], reduced PHM does not form stable adducts with molecular oxygen that can be studied spectroscopically in solution. Carbon monoxide can often act as a surrogate for molecular oxygen because of similarities in electronic structure that predispose it to bind at the same sites as O_2. Both molecules have lone pairs that lead to sigma donation, and empty π^* orbitals that have the correct symmetry to accept electrons *via* back-donation from a transition metal d-orbital manifold. The triple bond in the CO molecule arises from the presence of three empty antibonding orbitals, one sigma and two pi, whereas in O_2, only one of the pi-antibonding orbitals is empty. These differences lead to different geometric modes of coordination with O_2 binding either in a side-on or bent end-on configuration, and CO binding in a linear fashion. Notwithstanding, CO complexes are usually stable and provide comparative structural information *via* their infrared spectra. CO forms strong complexes with metal ions in low oxidation states *via* a strong sigma interaction of its lone pair with the metal ion coupled to overlap of its pi-antibonding levels with filled d-orbitals that back-donate electron density. Cu(I) with its d^{10} configuration forms strong complexes with CO (Table 1), generally *via* interaction of a 3-coordinate Cu(I) precursor complex with CO to form a 4-coordinate tetrahedral complex.[55–57] The back-bonding from metal to CO results in two noteworthy effects – first the strength of the C≡O bond weakens since electrons are populating its antibonding levels and this translates into a decrease in bond order and C≡O stretching frequency, and second, the magnitude of this effect and thus the observed frequency red-shift measured by Fourier transform infrared spectroscopy (FTIR) depends on the electron density residing on the metal ion which itself is strongly influenced by the other coordinated ligands. For example, since imidazole-N is more electron donating than thioether-S, histidine ligands decrease the ν(CO) more than methionine ligands. The magnitude of the red-shift is also expected to scale with the number of each ligand type in the complex.

CO binding to PHM and DBM. We exploited this chemistry to explore the reduced Cu(I) states of both DBM and PHM using FTIR and EXAFS spectroscopies (Table 1). Early experiments on DBM showed formation of a CO complex with ν(CO) of 2089 cm^{-1} relative to 2143 cm^{-1} for free CO in solution.[58,59] At the time the site of CO binding was unknown. In later work we explored the CO reactivity with bifunctional PAM[31] and the catalytic core of PHM.[60] For both these systems, the ν(CO) was 2093 cm^{-1} close but not identical to DBM. Using a chemical

Table 1 Carbon monoxide stretching frequencies for Cu(I) complexes of copper proteins and selected model compounds

Sample	Ligand set (excluding CO)	Coord. No (including CO)	ν(C ≡ O) (cm^{-1})	Ref.
DBM	$2N_{(His)}$ $1S_{(Met)}$	4	2089	58
PHM	$2N_{(His)}$ $1S_{(Met)}$	4	2093	60
PHM + AcYVG	$2N_{(His)}$ $1S_{(Met)}$	4	2093, 2063	60
PHM + Benzoylglycine	$2N_{(His)}$ $1S_{(Met)}$	4	2093, 2075	60
PHM M314H	$3N_{(His)}$	4	2075	36
PHM M314H + AcYVG	$3N_{(His)}$	4	2075, 2051	36
PHM H172A	$2N_{(His)}$ $1S_{(Met)}$	4	2092	75
PHM H172A + AcYVG	$2N_{(His)}$ $1S_{(Met)}$	4	2092, 2065	75
PHM H107A	$2N_{(His)}$ $1S_{(Met)}$	4	2092	36
PHM H107A + AcYVG	$2N_{(His)}$ $1S_{(Met)}$	4	2092	36
PHM H108A	$2N_{(His)}$ $1S_{(Met)}$	4	2093	36
PHM H108A + AcYVG	$2N_{(His)}$ $1S_{(Met)}$	4	2087	36
PHM H107AH108A	$2N_{(His)}$ $1S_{(Met)}$	4	2090	36
PHM H107AH108A + AcYVG	$2N_{(His)}$ $1S_{(Met)}$	4	2083	36
PHM H242A			No peak	36
CusF W44A	$1N_{(His)}2S_{(Met)}$	4	2108	73
CusF W44AM49H (M-site model)	$2N_{(His)}S_{(Met)}$	4	2089	71
CusF W44AM47HM49H	$3N_{(His)}$	4	2075	73
SeM CusF W44AM49H (M-site model)	$2N_{(His)}Se_{(Met)}$	4	2087	72
Aβ(10–14) YEVHH	$2N_{(His)}$	3	2110	39
Histidylhistidine (Nδ coordinated)	$2N_{(His)}$	3	2110–2105 weak	40
Histidylhistidine + *N*-methylimidazole	$2N_{(His)}N_{(imid)}$	4	2075 strong	40
HisXHis (X = Gly) (Nε coordinated)	$2N_{(His)}$	3	2092 strong	76
Hc (mollusk)	$3N_{(His)}$ + Cu–Cu	4	2062	77
Hc (limulus)	$3N_{(His)}$ + Cu–Cu	4	2053	77
Hc (arthropod)	$3N_{(His)}$ + Cu–Cu	4	2043	77
aa_3-cytochrome oxidase	$3N_{(His)}$ + Cu–Fe	4	2066, 2054, 2039	78
ba_3-cytochrome oxidase	$3N_{(His)}$ + Cu–Fe	4	2054	78
bis-dimethylimidazole ($[Cu\text{-}(Me_2imid)_2]^+$)	$2N_{(imid)}$		No reaction	79
Tris-dimethylimidazole ($[Cu\text{-}(Me_2imid)_3]^+$)	$3N_{(imid)}$	4	2069	79
Tris-(3,5-dimethylpyrazolyl)borate	$3N_{(pyrazole)}$	4	2081	80
Tris-(2-methylpyridyl)amine (TMPA)	$3N_{(py)}$ and $4N_{(py)}$	4 and 5	2094, 2075	81
1*H*-(imidazol-4-yl)-*N*,*N*-bis((pyridin-2-yl)methyl)ethanamine	$2N_{(py)}N_{(imid)}$	Probably 4	2082	81

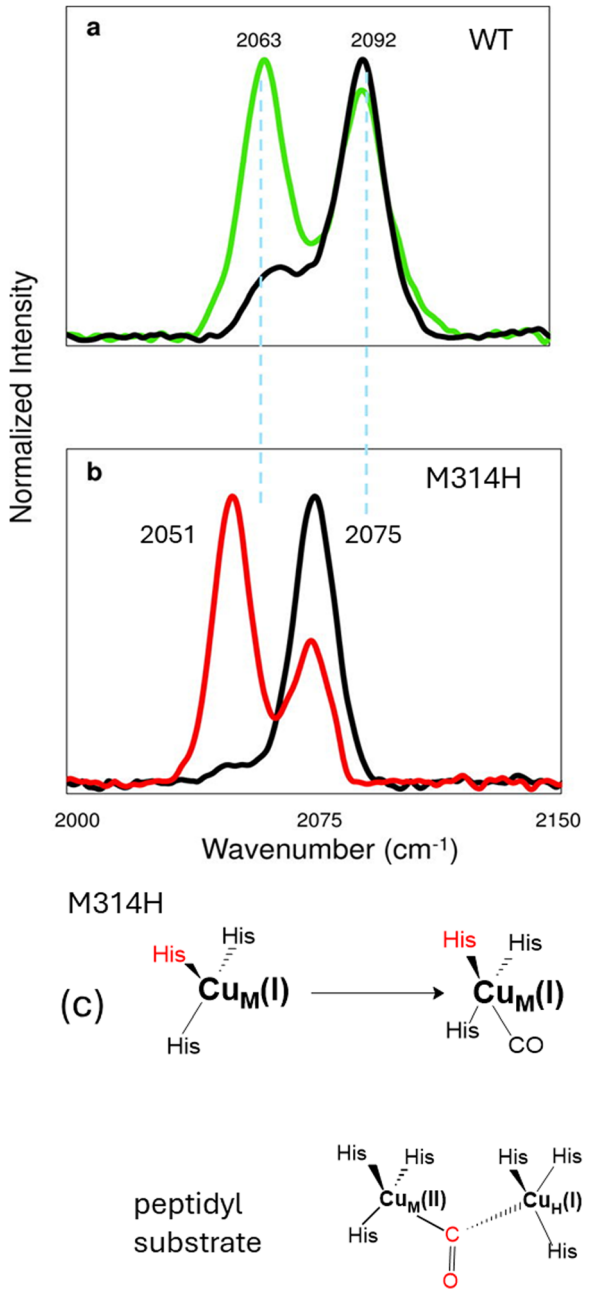

Fig. 4 CO chemistry of Cu(I)–PHM. (a) FTIR of substrate-free (2092 cm^{-1}) and substrate-bound (2063 cm^{-1}) enzyme. (b) CO complexes of the M314H variant showing both frequencies red-shifted by the Met to His substitution. (c) Suggested semi-bridged arrangement for the substrate-bound complexes.

assay based on the ability of deoxyhemoglobin (Hb) to compete-off the CO forming the HbCO adduct with λ_{max} = 420 nm, we were able to show that CO bound to only one of the Cu(I) sites in PHM. An important result was obtained when CO binding was repeated in the presence of substrate Ac-YVG where a second band was observed at 2063 cm^{-1} exhibiting a significant red-shift (Fig. 4). The new band implied activation of the site by CO binding such that the Cu center became more electron donating, suggestive of chemical activation for reaction with O_2. Titration with excess substrate did not lead to full conversion to the 2063 cm^{-1} species but rather produced an end point with each band near equal intensity. In later work[36] both 2093 and 2063 cm^{-1} bands could be assigned to reaction at CuM *via* studies on the M314H mutant. Here, substitution of histidine for methionine is expected to decrease the frequency on account of the increased donor power of histidine over methionine, and indeed ν(CO) for M314H was 2075 cm^{-1} but dropped to 2051 cm^{-1} in the presence of Ac-YVG. The fact that both frequencies decreased by large factors as the result of an M-site mutation allowed us to assign them both to different electronic/structural states of the CuM center.

The next question was how to interpret the 30 cm^{-1} red-shift induced by substrate binding. Curiously, no difference in coordination was observed by EXAFS at the M center. One possibility was a change in H-bonding interaction with the distal-N of coordinated His residues.[61] CuM ligand H242 is H-bonded to the side-chain amide of Q272 with a short 2.8 Å N···H···O bond. We tested whether strengthening this H-bond would decrease the frequency by making the imidazole of residue H242 more ''imidazolate-like''. A substrate-free Q272E variant gave a CO complex with ν(CO) of 2088 cm^{-1} insufficient to account for the magnitude of red-shift (unpublished data) but of greater consequence this frequency did not shift in the presence of Ac-YVG. H-site mutants had disparate effects. H172A showed a normal Ac-YVG red-shift but H107A and H108A showed no substrate effect. The data point to a substrate-induced structural change that activates the enzyme (providing complete coupling) and involves both the M site (red-shifted CO complex) and the H-site (requirement for either H107 or H108).

CO chemistry in a mononuclear M-site model system. A model system that mimicked the structure of the M-center and its reaction chemistry with O_2 and/or CO would be a useful tool for interpreting the CO reactivity of the PHM system. A number of inorganic model systems have been reported that contain N3 or N2S ligand sets and also react with oxygen at low temperatures (−120 °C) in organic solvents to form Cu(II)-superoxide complexes.[53,62–70] To test whether the same reactivity was observed in aqueous solution we built a protein-based model system by engineering a His_2S ligand set into the copper site of the small molecular scaffold CusF[71,72] (Fig. 5). The Cu(I) complex was exposed to air in the presence of sodium azide and the appearance of any Cu(II)-azido species was tracked at 390 nm. If the mononuclear Cu(I)His_2Met ligand set was reactive towards O_2 to form a Cu(II)-superoxo, azide should displace the $O_2^{-\bullet}$ which should then rapidly disproportionate in aqueous solution to O_2 and H_2O_2 leading to full formation of the Cu(II)-azido complex. We monitored the reaction for 24 h but observed no change in 390 nm absorption indicating that a Cu(I)–His_2S(Met) mononuclear complex required activation before it would form a cupric superoxide. In similar fashion to PHM, despite its lack of oxygen reactivity the model did bind CO giving rise to a Cu(I)His_2S(Met)CO complex that was characterized by EXAFS and FTIR. EXAFS gave a short 1.83 Å Cu–C(CO) distance, a linear Cu–C–O angle and a ν(CO) of 2089 cm^{-1}.

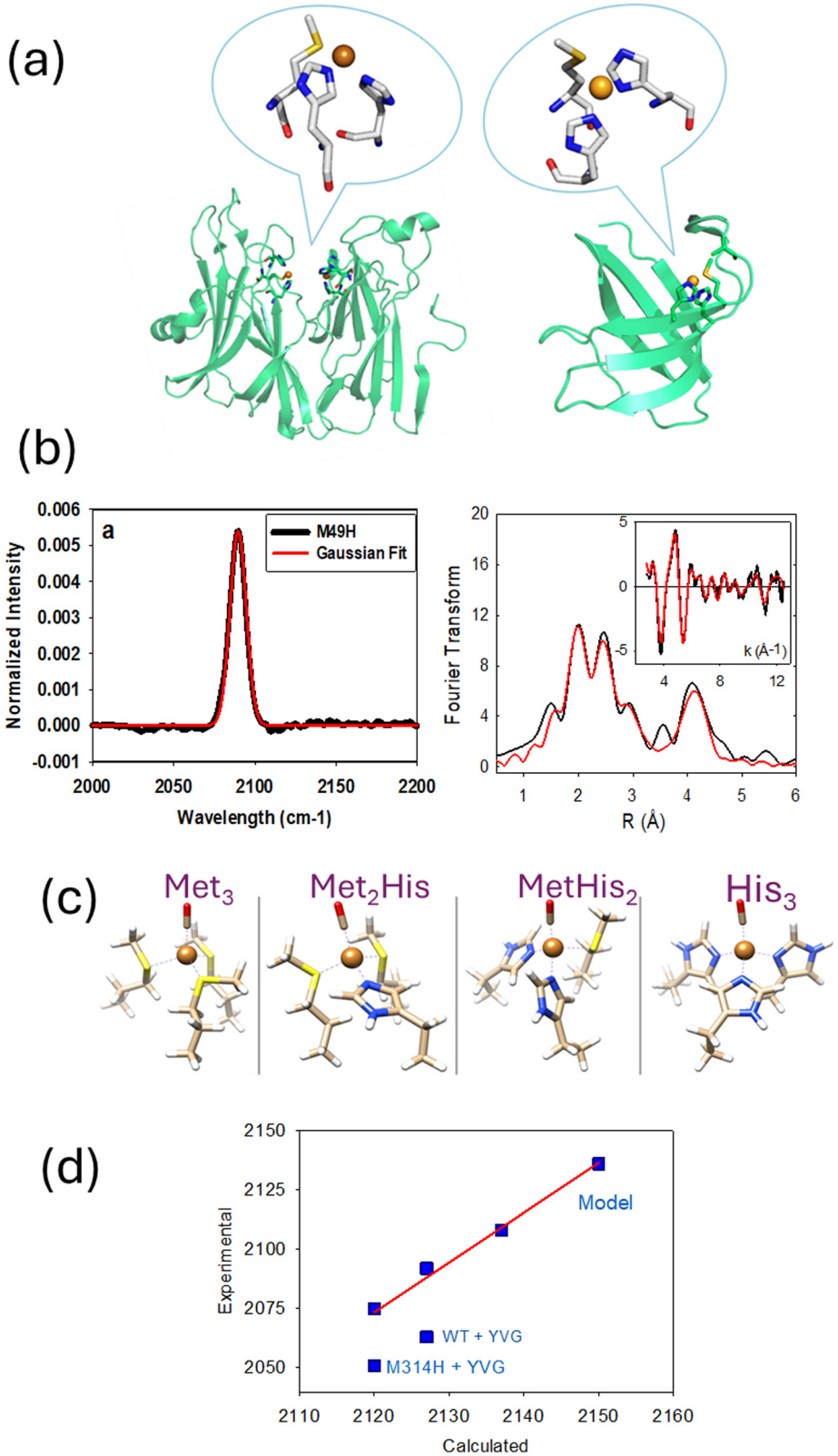

Fig. 5 An accurate protein-based model for the PHM M-site derived from the W44AM49H variant of the metallochaperone CusF. (a) Comparison of structural models adapted from pdb files 3PHM (reduced PHM) and 3E6Z (W44A CusF) respectively. (b) left panel FTIR and right panel EXAFS spectra for the complexes of the fully reduced M-site model with CO. (c) Geometry optimized structures for Cu(I)–CO complexes with variable His:Met ratios calculated using ORCA. (d) plot of experimental *versus* theoretical frequencies for the complexes in (c). Frequencies were calculated in ORCA.

Site directed mutagenesis also gave access to other ligand sets of general formula Cu(I)$(His)_x(Met)_y$ generating a series of Cu(I) complexes Cu(I)$(His)_3$, Cu(I)$(His)_2(Met)$, Cu(I)$(His)(Met)_2$ and Cu(I)$(Met)_3$. All but the Cu(I)$(Met)_3$ bound CO with frequencies of 2075, 2089 and 2108 cm^{-1} respectively. We compared these experimentally determined frequencies with those calculated by DFT to understand if the observed trends in CO vibrational frequency and EXAFS-derived bond distances could be correlated with frequencies and geometries using a minimal molecular model of each active site.[73] Initial models used WT CusF crystallographic coordinates (from PDB: 2VB2) including atoms from CusF His36, Met47, Met49, and the Cu atom, constraining the alpha-C atom of each residue to be located at its crystallographic position. The DFT procedure generated frequencies for Met_3 (H36M), Met_2His (WT), His_2Met (M49H), and His_3 (M47/49H) ligand sets which exhibited a linear relationship with the experimental data and established a faithful correlation between experiment and theory based on mononuclear coordination and standard treatment of electronic interaction of the CO ligand with each of the Cu(I)$(His)_x(Met)_y$ sites. Fig. 5(d) shows a plot of experimental *versus* computed frequencies for the engineered M-site model with the Ac-YGV red-shifted frequencies for WT and M314H PHM plotted for comparison. The substrate shifted frequencies are clearly anomalous and imply a large deviation from the inputs used for the model system.

Interpretation of red-shifted PHM frequencies. Mechanisms for red-shifted frequencies in Cu(I)–CO complexes have been attributed to various sources including (i) increase in N-donor (histidine) coordination number (ii) H-bonding between the distal NH of the imidazole of a His ligand and a protein-derived negative charge or dipole (iii) electrostatic coupling of the distal O of CO to a positive charge or dipole and (iv) a bridging or semi-bridging structure where the CO interacts with a second metal ion. The first of these has been discounted since ν(CO) for M314H +Ac-YVG drops well below that of the WT + substrate. Second, the Q272E mutant decreases the N–H–O hydrogen bond by 0.3 Å yet red-shifts the CO frequency by a mere 4 cm^{-1}.[74] Third, interaction of the CO distal O with a positive dipole as documented for heme carbonyls by Spiro and coworkers[82] is difficult to rationalize since Ac-YVG carries a *negative* charge at the pH of our experiments and therefore cannot increase the positive charge in the vicinity of the bound CO. Also, its binding interaction with the guanidinium group of R240 neutralizes the positive charge of the Arg residue. The final possibility that a conformational change leads to formation of a semi-bridging CO complex where the CO can interact with a second metal ion therefore seems most likely, particularly since the H-site ligands H107 and H108 appear important for the interaction. Indeed the frequency of the M314H Cu(I)–CO (2051 cm^{-1}) is lower than any frequency observed for a mononuclear Cu$(His)_3$ ligand set and is in the range observed for the CO complexes of the binuclear hemocyanins (2063–2043 cm^{-1}) where each copper has His_3 coordination[77] and where a semi-bridging mode was proposed as the origin of the lowered frequency (Table 1). Red-shifted IR frequencies are also observed in the CuB–CO complexes of cytochrome oxidase[78,83] between 2060 and 2036 cm^{-1}. Like hemocyanin, Cu(I)–CO frequencies below 2050 cm^{-1} appear to correlate with the presence of a second positively charged metal ion in the vicinity of the CO binding site. For cytochrome oxidase, the Cu(I)–CO species are formed by photodissociation of the CO ligand from the ferrous heme-a_3 with subsequent rebinding to copper. Interaction of the O atom with the positive charge of a second copper atom is therefore a plausible interpretation of the red-shift and would imply that activation is the result of an open to closed conformational transition.

Evidence for closed conformers and flexible sub-domain dynamics

The DBM structure. In 2016 Christensen published the first crystal structure for the homologous copper monooxygenase DBM.[15] Human DBM is a multidomain protein with a dimer interface that covalently couples two monomers *via* a disulfide bridge. Each monomer contains a catalytic core comprised of PHM-like CuH and CuM subdomains, a separate DOMON domain and a dimerization domain (Fig. 6). The dimer is asymmetric, and the two catalytic domains are present in two distinct conformations, one in which the CuH and CuM sites are separated and another in which the H domain has rotated about a residue in the interdomain linker to bring the CuH site closer to the CuM site giving rise to a closed conformation. Only one out of the 4 copper sites is partially occupied (CuM of the open conformer), but the unoccupied sites appear pre-organized for copper loading with identical ligand sets to those of PHM. Copper atoms can be modeled into these sites to give Cu–Cu distances for the open conformer of 14 Å and 4–5 Å for the closed conformer. The authors speculate that the closed conformer might represent the active state taking advantage of a coupled binuclear copper site for hydroxylation similar to tyrosinase[84] and catechol oxidase[85] while the open conformer might be used for loading substrates and release of products. A further suggestion posits that the DOMON and or dimerization domains could act as switches that would flip the structures from open to closed and closed to open in a synchronized fashion as necessary for active catalysis.

Closed conformers of PHM. For the ''open-to-closed'' mechanism for DBM to be considered, similar conformational dynamics must exist for PHM. This is because it has been established through measurement of identical primary deuterium KIEs for the two enzymes that they must have close to identical transition states.[43,86] At the time of publication of the DBM structure all published PHM structures had invariant Cu–Cu distances of 11 Å. However, in 2018 a number of PHM structures of H-site variants were reported.[87] One of these, the H108A variant crystallized in the presence of citrate showed a closed structure with a near identical arrangement of the H and M subdomains to those of the closed conformer of DBM (Fig. 7). However, this structure contains only a single copper atom coordinated by His residues H242, H244 from the M-site and His residue H107 from the H-site. A bidentate citrate molecule completes the 5-coordinate Cu(II) ion which is

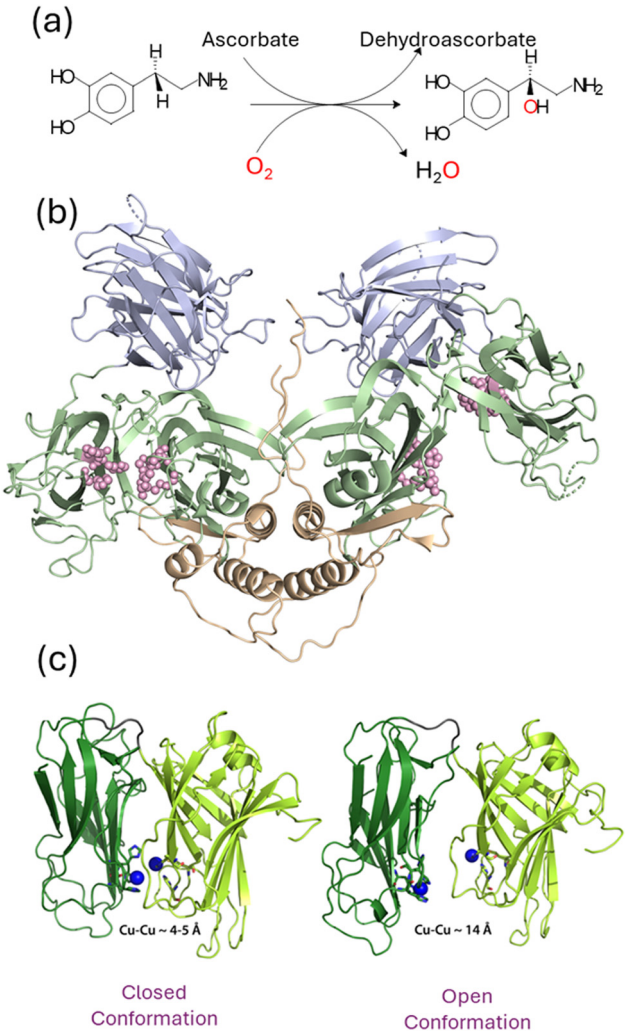

Fig. 6 (a) Reation catalyzed by dopamine β-monooxygenase (DBM). (b) Structure of DBM showing the three domains: catalytic domain in green, doman domain is slate blue, and dimerization domain in gold. The active site residues in each of the catalytic domains are shown as pink spheres with the closed domain on the left and the open domain on the right. (c) Representation of the closed (left) and open (right) structures for the catalytic domains with Cu–Cu distances of ~4 and 14 Å recpectively.

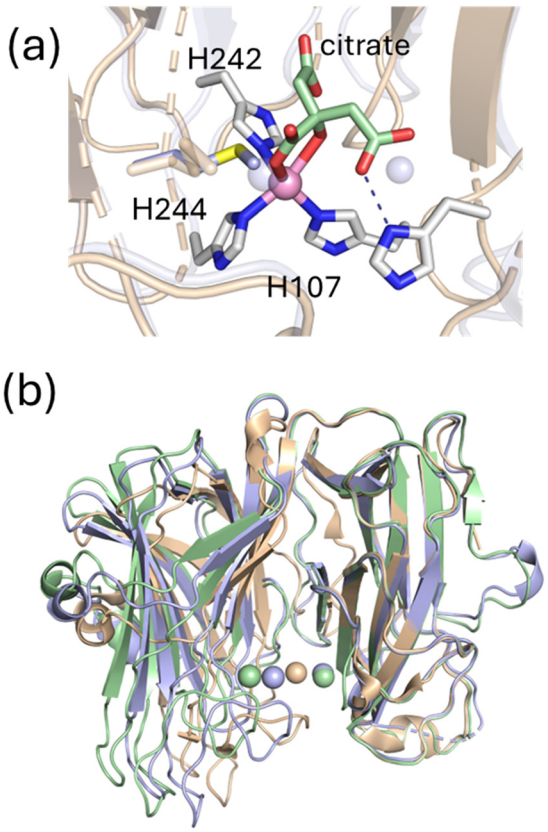

Fig. 7 (a) Structure of the H108A variant of PHM in the presence of citrate pdb 6ALA. The single Cu(II) ion is shown as a pink sphere bound to H242, H244, and H107. A bidentate interaction with citrate completes the 5-coordinate structure of the Cu(II) ion. The positions of the Cu atoms in the oxidized structure (Cu–Cu = 11 Å, 1PHM) are shown as transparent spheres (b) Overlay of H107A + citrate (closed, gold, 6ALA), oxidized (Cu–Cu = 11 Å, slate, 1PHM) and oxidized anaerobic (Cu–Cu = 14 Å, green, 8DSJ) with the structures aligned on the H domain.

displaced from its position in WT such that the Met314 residue is uncoordinated and at >5 Å from the copper atom. While this structure is clearly non-catalytic it shows that there is no impediment for interdomain movement between the two subdomains in PHM.

Fully open conformers of PHM. Two other structures relevant to PHM interdomain dynamics were published from our laboratory in 2023.[61] The first of these was the Cu(II)-loaded form of the Q272E variant while the second was that of WT crystallized under anaerobic conditions. These were notable in that they represented interdomain movement in the opposite direction leading to structures with Cu–Cu of ~14 Å. Otherwise, the structures were similar to WT and individual sub domains aligned well with those of WT with RMSD values of ~0.3 Å. When these new structures were analyzed against WT and the H107A/citrate structures a simple relationship became evident. The structures were all related by different degrees of rotation about an axis through residue Ile201 which resides in the linker region between the two subdomains. Rotation in one direction resulted in the CuH site moving closer to CuM while rotation in the opposite direction increased the Cu–Cu separation (Fig. 8). The crystallography suggests that Cu–Cu of ~4.5, 11, and 14 Å may represent states of special stability, but there appears little impediment to interdomain movements that could lead to other Cu–Cu separations, or indeed to facile interdomain movements as an integral part of a catalytic cycle.

A new open-to closed mechanism for DBM catalysis from QM/MM calculations

For an open to closed transition to be mechanistically feasible, it would have to proceed with an activation energy lower than that required for HAA chemistry. Wu *et al.*[49] have recently explored the energy landscape for such a mechanism for the reaction of DBM with hippuric acid using a QM/MM approach. The starting point for comparing the energetics of an open mechanism with one involving domain closure is assessing the

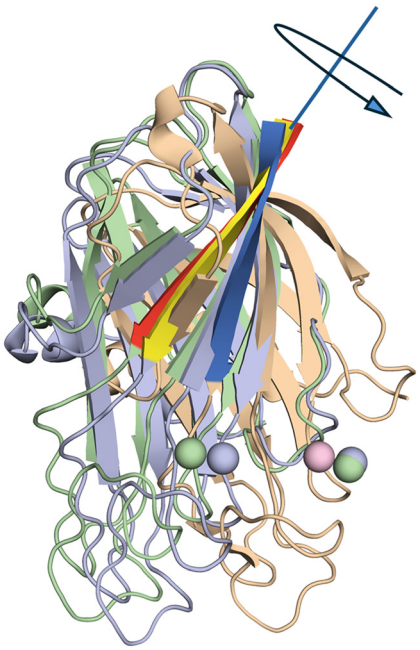

Fig. 8 Mechanism for closed to open transition involving rotation of the M domain relative to the H domain about an axis or hinge that bisects residue Ile 201 in the loop connecter between the two sub domains. The beta strand that facilitates this rotation is shown as red for the fully open structure (Cu–Cu = 14 Å) yellow for the partially open structure (Cu–Cu = 11 Å) and dark blue for the closed structure. Cu atoms are shown as spheres color coded green for fully open, slate blue for partially open, and pink for closed.

reactivity of the CuM(II)–$O_2^{\bullet}$ cupric superoxo species in the open conformation. An important premise of the work is that excess ascorbate is present during catalysis such the cupric superoxo has the choice of abstracting a H atom from bound substrate or from the ascorbate $HAsc^-$ anion which is freely accessible to the active site. Energy calculations suggest that HAA from ascorbate (10.2 kcal mol^{-1}) is more favorable than HAA from hippuric acid (DBM, 26.1 kcals mol^{-1}) or formylglycine (PHM, 22 kcals mol^{-1}) by a large amount making the formation of a Cu(II)M–OOH hydroperoxide and ascorbate radical a more likely outcome. They further calculate that the energy of H_2O_2 formation *via* dissociative protonation (8 kcal mol^{-1}) exceeds that for domain closure (DBM,1.3 kcal mol^{-1}; PHM, 2.1 kcals mol^{-1}) suggesting that once formed the Cu(II)M–OOH species would undergo domain closure rather than release the hydrogen peroxide ensuring that the reaction would remain completely coupled. Domain closure leads to formation of the *mixed valence* binuclear complex μ-OOH–Cu(II)MCu(I)H that undergoes internal ET from Cu(I)H to break the O–O bond and form an oxyl-bridged HOCuM(II)–($O^{\bullet}$)–CuH(II) species capable of HAA from the bound substrate. OH radical rebound, domain opening and further ascorbate reduction and substrate binding to the open conformer complete the catalytic cycle.

Like the canonical mechanism discussed earlier this mechanism predicts primary and secondary KIE values for the chemical step that are comparable with experiment, but otherwise its predicted intermediates remain unverified. Notwithstanding, the role of ascorbate as the initiator of the process leading to domain closure is testable. In a series of experiments we examined the role of ascorbate in pre-steady-state single turnover reactions of PHM using dansyl-YVG as substrate.[30] The enzyme was first reduced with ascorbate, and the excess ascorbate removed anaerobically. This ascorbate-free preparation was then reacted with dansyl-YVG and O_2 and the reaction quenched at appropriate times using rapid chemical quench methodology. Hydroxylated product was determined by HPLC separation and fluorescent detection to obtain rates and stoichiometries of product formation with the expectation that the ratio of product formed to reduced enzyme starting material would approach unity at the end point of the single turnover. Surprisingly, ascorbate-free reduced enzyme generated <15 percent of the expected hydroxylated peptide, with the result confirmed for the extent of enzyme copper oxidation by RFQ (rapid freeze quench) EPR spectroscopy. The ratio could be increased to about 70 percent if ascorbate was added back to the reaction mixture in a process that was proven not to be due to multiple turnovers. Measurement of reaction rates as a function of ascorbate concentration indicated saturating behavior with a K_D for ascorbate of 117 μM an order of magnitude less than the K_m measured from steady state suggesting a role distinct from Cu(II) reduction. The most intriguing aspect of ascorbate activation was a correlation between ascorbate concentration and the intensity of the 2063 cm^{-1} substrate induced Cu(I)M–CO band (*vide supra*) when the latter was formed by CO reaction with an ascorbate-reduced di-Cu(I) sample of PHM. This result suggested that the mode of activation might correlate with the open-to-closed transition (Fig. 9).

Capturing a fully metalated binuclear state in solution

Design of a bifunctional peptidyl "Lure" and formation of a binuclear mixed-valence species. Evidence for a binuclear state presented so far has been derived from crystallography and inferred from interpretation of kinetic and spectroscopic data. We were therefore eager to devise a methodology to stabilize the binuclear state in solution in a fully metalated form that could be characterized by structurally-focused techniques such as EPR and XAS. We used the peptidyl inhibitor Ala–Ala–Phe-homocysteine (AAF-hCys) known to form a strong complex with the enzyme[88] with the expectation that binding might occur both *via* the C-terminal carboxylate salt bridge to R240 and *via* additional coordination of the thiol to copper. Binding to both coppers would establish the existence of a conformer in the closed binuclear state. Titration of ~2 equivalents of peptide into oxidized PHM resulted in an intense purple coloration with a unique UV/vis spectrum (Fig. 10) showing a broad band centered at 925 nm and weaker bands at 580 and 460 nm.[89] The 925 nm feature was assigned as an intervalence charge transfer transition (IVCT) reminiscent of mixed-valence (MV) centers such as those found in CuA of cytochrome oxidase (460, 530, 795 nm)[90] and an associated bis-thiolate model system (358, 602, 786, and 1466 nm).[90,91] The CuA site in subunit 2 of CCO is

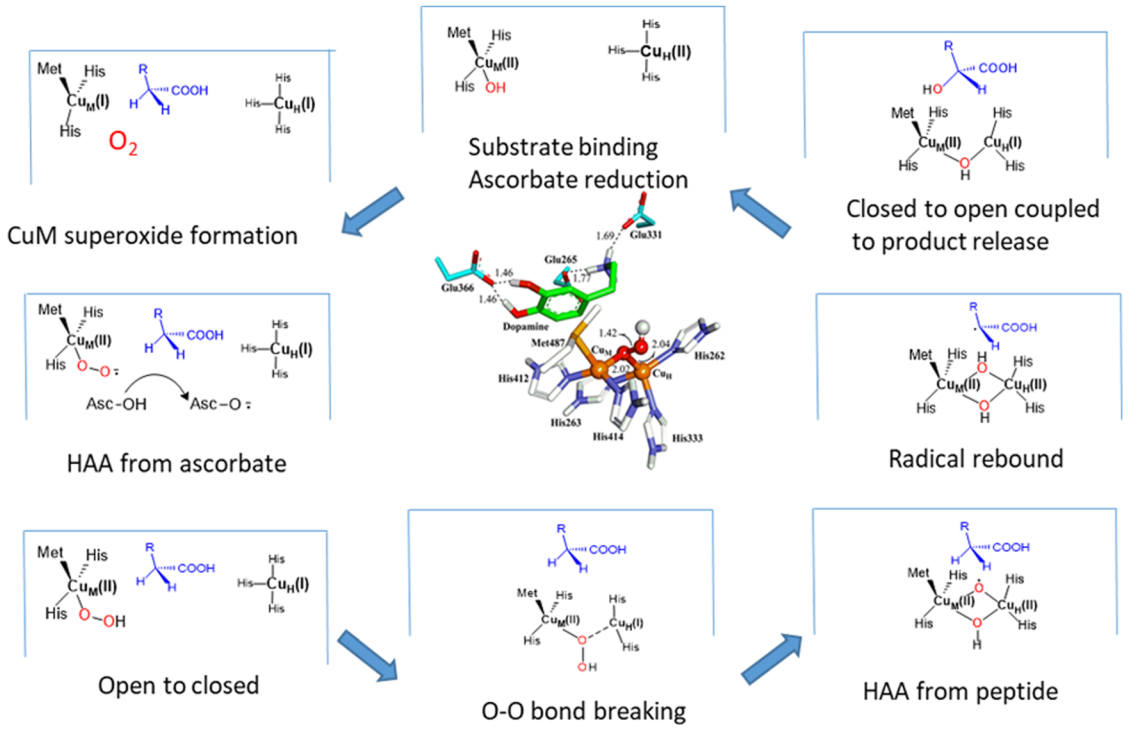

Fig. 9 A new mechanism derived from QM/MM calculations based on a conformationally gated open-to-closed catalytic cycle. The structure of the proposed intermediate mixed-valence intermediate is shown in the center of the figure. Figure constructed from concepts proposed in ref. 49.

a diamond core structure composed of a pair of coppers bridged by two cysteine thiolate residues with a single histidine residue coordinating each copper in a terminal fashion and weakly bound axial ligands (Met and amide oxygen) completing the coordination sphere. The single unpaired electron is shared equally between the two coppers generating a fully delocalized mixed-valence system. In the PHM system EPR (*vide infra*) indicated that the purple complex was ~50 percent reduced. The reducing equivalents required to generate a Cu(I) component must come from the homocysteinyl thiolate being converted to a disulfide in a "sacrificial' reaction in a similar fashion to that of CuA reconstitution from Cu(II) ions which likewise uses thiol ligands as the source of the necessary electron.[92,93] This explains why at least two equivalents of peptide are needed to fully form the complex.

Despite these similarities the PHM MV complex appears structurally distinct. The CuA system is a fully delocalized $Cu^{(1.5+)}Cu^{(1.5+)}$ species (class III) MV complex,[90,94–96] and is found in a variety of other systems, including N_2O reductase,[97–99] purple copper azurin,[100,101] and pMMOD[102] while the PHM complex is valence localized. The canonical CuA site exists as a pseudo planar $NCuS_2CuN$ diamond core with a 7-line Cu-hyperfine pattern in the EPR spectrum that implies full electron delocalization. The extremely short Cu–Cu distance (2.4 Å) facilitates the delocalization *via* direct Cu–Cu bonding where the dimer-coupled $d_{x^2-y^2}$ orbitals form a σ_u^* HOMO with a direct sigma interaction along the Cu–Cu axis. The PHM system on the other hand gives rise to an EPR spectrum which shows a 4-line pattern typical of what is termed a class II mixed valence system where the unpaired electron localizes onto one of the copper centers. In this respect it is more similar to the halide-bridged complexes of half-met hemocyanin[103] which exhibit intervalence transitions above 900 nm but 4-line rather than 7-line Cu-hyperfine patterns indicative of spin localization with Cu–Cu distances of ~3–4 Å based on known structures of oxy and deoxy hemocyanin.[104,105] In PHM the spin localization is likely due to the presence of only one bridging thiolate in contrast to the two thiolate bridges and Cu–Cu bond found in CuA.

The binuclear reduced state. The presence of a single thiolate bridge was fully confirmed in the complex formed between the AAF-hCys peptide and the fully reduced Cu(I) PHM. EXAFS data on WT protein showed strong Cu–S scattering from >1 S ligands per Cu(I). Importantly, the M314H variant gave an EXAFS spectrum that simulated to 0.9 Cu–S per Cu, removing the ambiguity associated with the competing scattering from Cu–S(hCys) and Cu–S(Met314) interactions. Further studies using a selenium-substituted homocysteine peptide (AAF-hSeCys) confirmed and extended these conclusions from XAS data collected at both the Cu and Se absorption edges.[106] For the fully reduced di-Cu(I) species, the characteristic signature of a bridging selenide was obtained with the Se data showing close to 2 Cu *per Se* and the Cu data showing close to 1. The seleno-complex also formed a class II IVCT which like the S-analogue gave EPR data that were consistent with a localized mixed valence species since the spectrum showed a 4-line pattern in the parallel region. Taken together the data

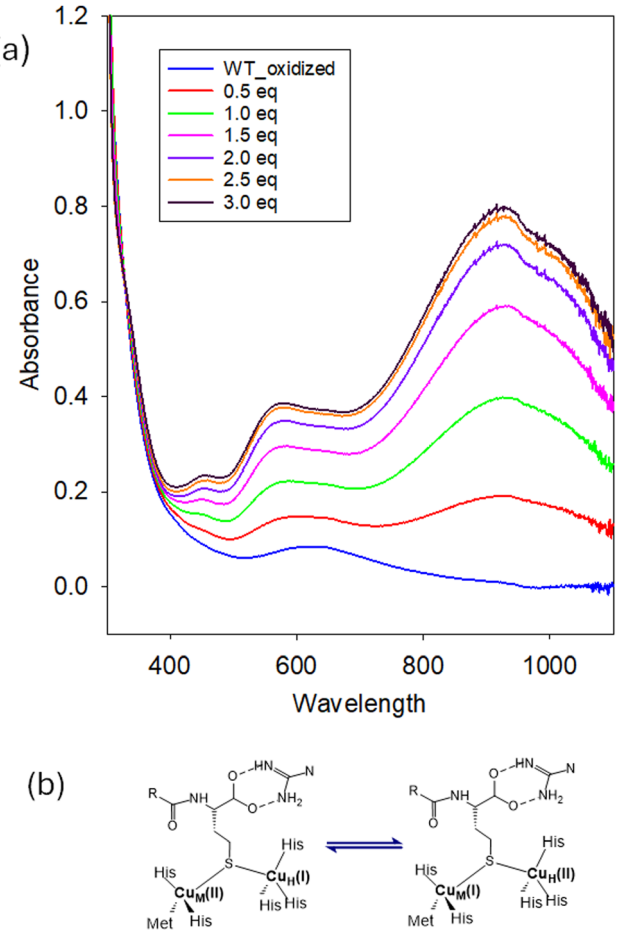

Fig. 10 (a) Titration of oxidized PHM with the AAF-hCys peptide. (b) Suggested mixed valence species responsible for the broad absorption around 925 nm.

point strongly to the formation of a S/Se-bridged binuclear species.

The stability of the MV complexes of the AAF-hCys/hSeCys with PHM is remarkable. For the S-containing homocysteine peptide the deep purple color of the MV complex is stable indefinitely at room temperature, and bleaches over a period of hours when exposed to ascorbate as a reductant. The seleno complex is reduced faster which is anticipated for a selenolate complex.[107,108] However, stable MV complexes are generally utilized for specific functions in metalloproteins. The CuA systems described above are used to accelerate long range electron transfer, as (with a few notable exceptions) are iron–sulfur clusters. The proposal (*vide supra*) for a catalytic MV peroxo intermediate adds significance to the PHM MV complex: although certainly off-pathway, the mono-bridging thiolate complex is likely to have a geometry that mimics the proposed μ-1,1-peroxo intermediate, and demonstrates that a conformation that could accommodate the intermediate is possible. One may speculate that the enzyme could supply a bridging group such as imidazole from histidine or OH from serine/threonine that might help stabilize a MV intermediate during catalysis.

We suggested a plausible mechanism for domain closure in PHM based on simple electrostatics.[61] The oxidized enzyme in the absence of substrate contains five positive charges in the active site cleft which are subject to modification by reduction and substrate binding. These include two each from the Cu(II) centers and one from the guanidinium group of Arg240. When the enzyme is reduced and binds substrate the positive charge is reduced by 3, as the substrate forms its salt bridge with R240 and the Cu atoms are reduced to Cu(I). If ascorbate binds in the active site pocket as $HAsc^-$ this would reduce the net positive charge to 1. Given the energy for domain closure is a mere 2 kcal mol^{-1}, the decrease in electrostatic repulsion between the two sub-domains as the result of this decrease in net positive charge could be sufficient to induce domain closure. It is worth noting that this mechanism would not work as well for DBM where the substrate dopamine in uncharged. However, as noted above DBM may utilize a distinct pathway for domain closure orchestrated by allosteric effects in either the DOMON domain or dimerization domain or both, which may result in the two catalytic cores of each active dimer to exist in asymmetric open and closed conformers. This would explain why monomeric DBM protomers appear to be inactive.

Ribosomally synthesized and post translationally modified peptides (RiPPs)

Radical SAM RiPP chemistry

We turn next to systems that generate natural peptide products that have gained function through post-translational modification. The more common examples of this class of bioactive molecules are derived from non-ribosomal peptide synthesis (NRPS) and will not be discussed further. Here we will examine metal-mediated peptide transformations in the ribosomally synthesized and post-translationally modified peptides or RiPPs which encompass a large class of bioactive molecules produced by all classes of microorganisms often with specific antimicrobial properties that suggest importance in host defense. There are many subclasses of RiPPs with diverse function[4] where the enzymatic products include nisin (an antibacterial food additive), bottromycin (active against MRSA) and plantazolicin (active against *B. anthracis*) as specific examples. Of interest to this review are RiPPs containing thioether crosslinks such as the antibacterials subtilosin A and thuricin H where a cysteine S of the substrate peptide reacts at an activated C atom catalyzed by the associated maturase. The advent of inexpensive genome sequencing has aided the discovery of these systems since the substrate peptide and its associated maturase are generally clustered in the same operon and can be identified by data mining techniques.

Sactipeptides and ranthipeptides[4,109,110] contain thioether crosslinks between a cysteine S and the alpha, beta or gamma C of another amino acid. The maturases PapB, Tte1186 and CteB are homologous radical SAM (RS) enzymes that catalyze thioether crosslinking reactions using the RS cluster together

with two additional FeS auxiliary clusters all of which are essential to the crosslinking reaction.[8,111] The radical SAM cluster is a site-differentiated FeS cluster where one out of the four Fe atoms binds the *S*-adenosylmethionine cofactor *via* the α-amino and α-carboxylate of the methionine. The reduced form of the cluster initiates reductive cleavage of the coordinated SAM moiety to form a 5-deoxyadenosyl radical Ado• which is capable of HAA from the peptide substrate to form a peptidyl substrate radical. In the case of sactipeptide thioether crosslinking reactions the cysteine-S must then couple with the radical in a process that also requires an electron and a proton. The absolute requirement for both auxiliary clusters in completing the chemistry points to their mechanistic importance but does not immediately suggest how it is achieved.

The crystal structure of CteB from *Clostridium thermocellum* provides some insight into the function of the auxiliary clusters and their interaction with the RS cluster.[112] CteB has an RS-SPASM structure where the RS cluster is located in a characteristic triosephosphate isomerase (TIM) barrel, with the two auxiliary clusters AC1 and AC2 located in a separate C-terminal cysteine rich domain called a SPASM domain. Interestingly, the structure of CteB with its peptide substrate shows an interaction between an Fe atom in AC1 and a cysteine-S of the substrate, although this Cys (C21) is not the one that forms the crosslink (C32). However, this structure suggests that a function of the auxiliary cluster might be to bind and activate the reactive cysteine while its proximity to AC2 might provide a conduit for transfer of the second electron needed to complete the reaction. The structure of the CteB homologue and its substrate complex is shown in Fig. 11.

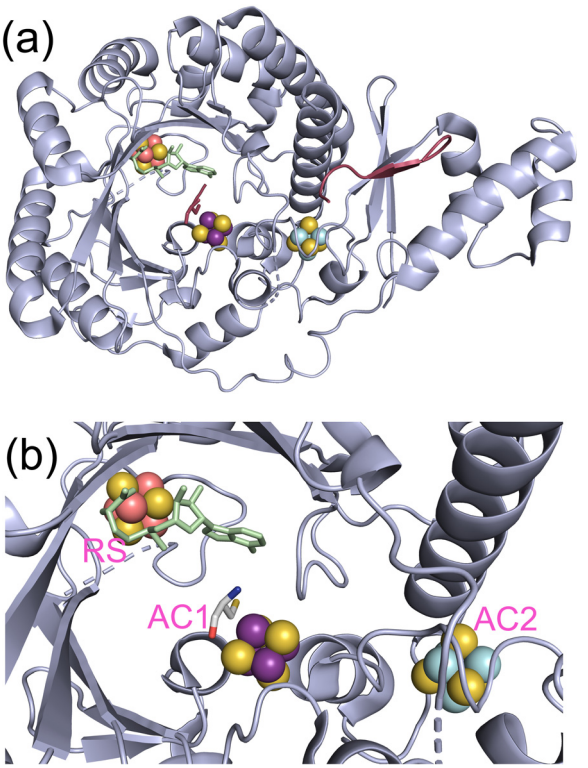

Fig. 11 Structure of the radical SAM (RS) RiPP maturase CteB. (a) Full length protein showing TIMM and SPASM domains with bound peptide shown as a salmon strand. (b) Close up of the cluster region showing the RS cluster (Fe atoms in orange), AC1 cluster (Fe atoms in purple), and AC2 cluster (Fe atoms in cyan). From pdb file 5WGG. The cysteine bound at AC1 is C21 rather than the crosslinking C32 residue.

We used the concept of substrate coordination to an Fe atom of an auxiliary cluster to design an experiment that would provide spectroscopic evidence for this mode of action.[8] Using the peptidyl substrate for PapB (C19U msPapA) we substituted the reactive cysteine for selenocysteine and then showed that in the presence of PapB, SAM and sodium dithionite this homologue underwent enzyme-dependent reaction to form a selenoether *via* crosslinking to a residue between positions 19 and 23, similar to what had been reported for the Cys-containing peptide. Next we examined the EXAFS of the PapB-C19UPapA complex at the Se edge which indicated strong scattering between the Se absorber and an Fe atom of one of the clusters (Fig. 12). Of significance, samples prepared under catalytically active conditions showed an increase in the intensity of the Se-C peak in the Fourier transform, indicating that selenocysteine (1C *per Se*) had undergone partial conversion into the selenoether (2C *per Se*). We could then use cluster-deletion variants of the Tte1186 homologue to localize the binding to auxiliary cluster 1 which is expected to occupy a position analogous to that shown in the CteB structure. This work highlighted the role of a site-differentiated Fe center in the auxiliary clusters in RS RiPP maturases for both peptidyl substrate binding and potentially catalytic activation, where electron donation from the cluster increases the electron density on the thiol/selenol for radical coupling to a carbon-based radical on a nearby residue generated by reaction with Ado•. It is possible, perhaps likely, that auxiliary cluster 2 might aid in this activation process *via* supplying the electron necessary to complete the radical coupling.

Copper mediated RiPP chemistry

An emerging class of RiPPs that install tryptophan and tyrosine crosslinks has been described in plants[1,11] and more recently in fungi.[12] The plant systems termed BURP domains or burpitide cyclases (BpCs) are unusual since often a single open reading frame codes for both peptide substrate (core peptide) and its maturase, such that the ribosomally encoded precursor is autocatalytic and destroys itself during the formation of the RiPP products. The cyclization reactions require copper atoms, and unlike the radical SAM dependent enzymes that function under strict anaerobiosis, the BpCs appear to utilize oxygen in their catalytic chemistry.

In 2024 Kersten, Mydy and coworkers reported the first crystal structure of a BpC, the AhyBURP domain reconstituted with Cu(II). The structure revealed new Cu-dependent RiPP chemistry involving indole-N and tyrosyl-O coupling to an unactivated C in the core peptide.[10] The core peptide has the sequence Q^{79}PYGVYTW^{86} and undergoes autocatalytic

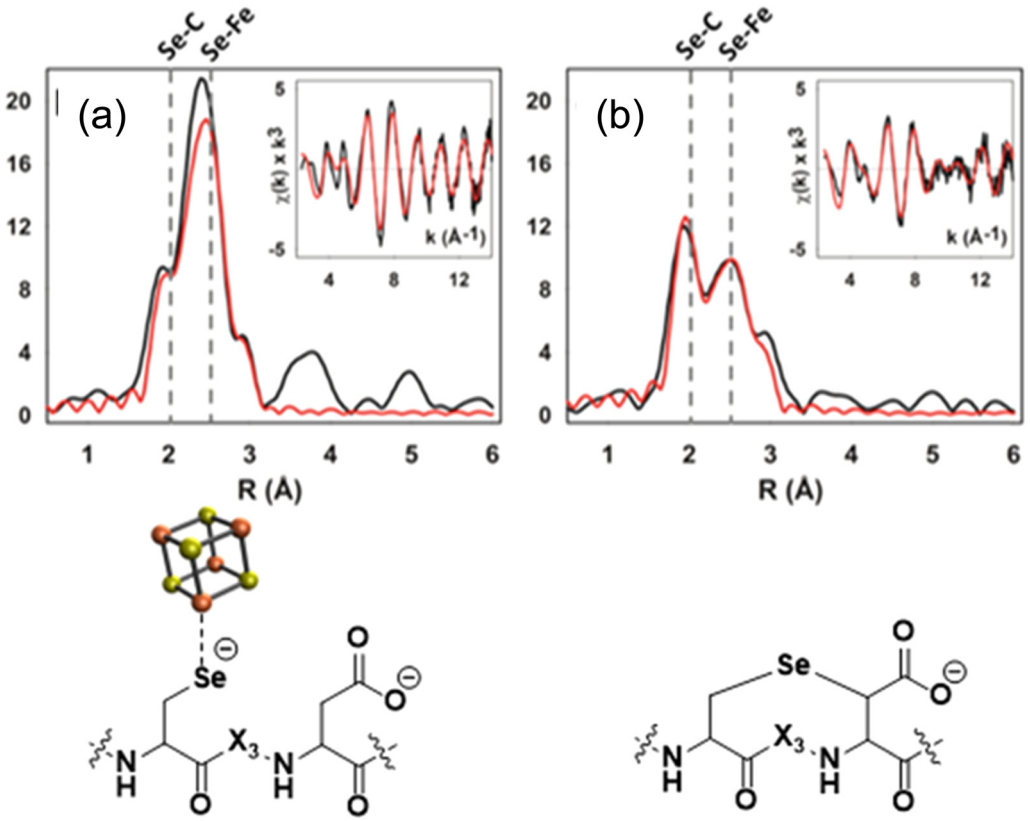

Fig. 12 Se edge EXAFS of PapB reacted with a SeCys-substituted substrate peptide. (a) An intense Se–Fe peak is observed at 2.4 Å when peptide is added in the absence of SAM and DTT. (b) Reaction in the presence of SAM and DTT shows an increase in the Se–C and decrease in the Se–Fe as peptide is converted into the crosslinked product.

processing to form two crosslinks, one between G82 and W86 to form lyciumin, and the second between Q79 and Y84 to form the double macrocycle legumenin (Fig. 13). The structure of AhyBURP has a novel protein fold and an active site comprised of two Cu atoms that face each other across a 7 Å wide cleft (Fig. 13). Each Cu center is built from a Cys–His repeating motif –(CH–X_n)$_4$- creating a bis-histidine binding site, stapled on the backside by a disulfide formed from the Cys residues. The Cus are flanked by conserved Met residues that are positioned at too long a distance to be Cu(II) ligands but may potentially bind to the Cu(I) form. The core peptide straddles the cleft and the amide oxygen of Gly82, the residue destined for a crosslink with W86 in the first cyclization, forms a weak bond with one of the Cu centers. The disulfide staple appears to constrain the His residues to be *cis* to one another, a strategy that could potentially prevent them from attaining a preferred linear coordination in the Cu(I) form and opening up a vacant coordination position for oxygen binding. Both sites are required for autocatalysis, since His to Ala mutations at any of the His residues abrogate peptide crosslinking. Mutagenesis of the core peptide itself is consistent with initial formation of the W86 to G82 crosslink followed by a sequential cyclization that couples Q79 with Y84. It is also apparent that some chemistry can still persist with core peptide mutants that lack the native crosslinking residues, often leading to Y81–Y84 crosslinks suggestive of radical coupling initiated by the copper center itself. The authors used a novel radical trap (CHANT) capable of trapping short lived radicals to capture a transient radical associated with the core peptide residues Y81–W86, consistent with radical formation in the first cyclization. Together their data supported an active site comprised of a pair of Cu(His)$_2$ centers that react with oxygen to form an oxy-intermediate capable of hydrogen atom abstraction from a residue in the core peptide followed by radical coupling of G82 and W86. The process is then repeated in a second cyclization that crosslinks Q79 and Y84.

It is hard not to notice the strong similarity between the active site structure of the Cu centers in AhyBURP and the Cu centers particularly the CuM center of PHM. As described earlier in this review, PHM generates a glycine radical *via* oxygen chemistry at its homologous Cu(I) His$_2$Met site and in another unusual twist, the Met residue coordinates Cu only in its Cu(I) state. The understanding of the reaction chemistry of BpCs is still in its infancy, yet it is intriguing that the Cu centers in the crystal structure of AhyBURP appear to be placed at a distance in between the open and closed conformers of PHM and DBM. While too early to speculate, it seems at least a possibility that the reaction chemistry of BpCs may also utilize open and closed conformers and/or binuclear states.

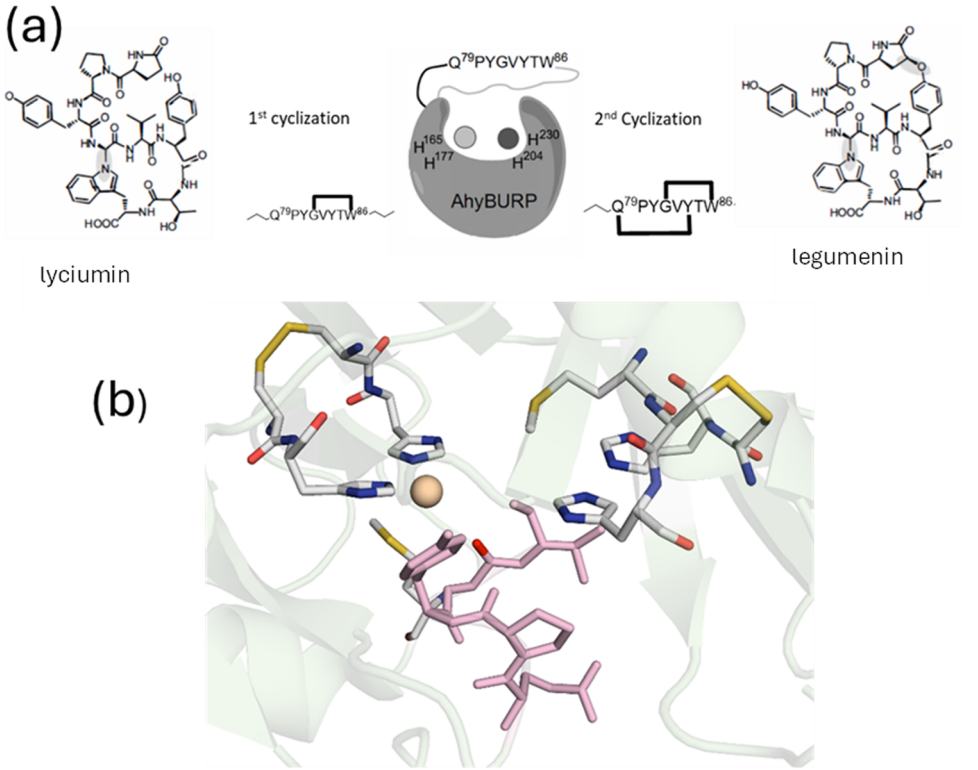

Fig. 13 Copper-mediated RiPP chemistry. (a) Crosslinking reactions of the the AhyBURP protein. (b) Crystal structure of Cu(II)AhyBURP showing coordination of a Cu ion in its bis-His site. The core peptide is shown in pink from pdb file 8SY3.

Conclusions

Posttranslational peptide processing generates important products that benefit the organism whether as neuropeptide signaling molecules or cyclic derivatives that assist in host defense. The one-electron redox chemistry inherent to metal ions such as copper and iron provide mechanisms for generating peptidyl radicals that act as intermediates for both amidation and crosslinking reactions.

For the copper-mediated peptide amidation, we have reviewed evidence that is beginning to challenge the canonical "mononuclear" mechanism in favor of one proceeding through a binuclear and possibly mixed valence intermediate. The canonical mechanism was based on two tenets – first that the Cu–Cu distance was invariant and second that the reaction was initiated by a CuM–dioxygen complex and could proceed to products within the crystal implying that it retained the conformation observed in the structure – *viz* an open conformation – throughout the catalytic cycle. Revisiting the mechanistic landscape after the premise of invariant sub-domain separation had been disproved, led to the formulation and later discovery of states with binuclear configurations. Both mechanisms account equally well for the observed reaction energetics and kinetic isotope data, but the binuclear mechanism is better able to accommodate a number of other experimental findings. For example, contrary to expectation from model studies in organic solvents at low-temperature O_2 was unreactive towards our water soluble mononuclear M-site 5protein analogue built from the CusF scaffold emphasizing the need for enzyme activation. Additional evidence not previously introduced includes peroxide-shunt chemistry[113] where product could be formed catalytically from oxidized PHM and hydrogen peroxide but led to 60 percent O isotope scrambling with ambient O_2 in the hydroxylated product when $H_2{}^{18}O_2$ was used as the source of O in the product. This result required the reaction to cycle through an intermediate where a Cu(II)-peroxide or hydroperoxide is in equilibrium with a Cu(I) dioxygen species and strongly suggested the intermediacy of a species similar to that of the binuclear copper centers of hemocyanin and tyrosinase, as also discussed for the origin of the substrate-induced red-shifted M-site CO band. Lastly we noted the unusually large effect on the rate of HAA from the H172A mutant suggesting that the ligand H172 at CuH has a major effect on the structure of the transition state located at CuM.

The essential role of Met314 in PHM catalysis is an experimental finding that has been difficult to rationalize by either mechanism. The canonical mechanism relies on conclusions from Cu(II)-superoxo reactivity that seem to suggest that thioether coordination enhances the HAA potential of the cupric superoxo. For example a recent study of the $[(^{TMG}N_3S)Cu^{II}(O_2{}^{\bullet-})]^+$ CuM model superoxo complex found an increase of $\sim$1.5 fold in the second order rate of HAA with the TEMPOH substrate over the analogous $[(^{TMG}N_4)Cu^{II}(O_2{}^{\bullet-})]^+$ species.[114] The difference in rate between N- and S- coordinated complexes is small, and certainly insufficient to account for that observed in the enzyme. Wang *et al.* on the other hand

explain the M314H result by calculating an O–O cleavage barrier 3.1 kcal mol^{-1} higher than that for the WT.[49] At a qualitative level one may speculate that the highly fluxional and weakly bound Met residue[71,72] may facilitate the necessary movement to the CuM atom as it toggles between open and closed states, and indeed the S(M314) thioether sulfur is displaced by almost 3 Å away from the copper center in the closed H108A structure.[87] The more strongly bound His residue may be energetically restrained from accommodating this movement.

The similarities in both ligand-set and dioxygen-induced peptide radical formation argue forcibly for mechanistic correlations between PHM and BpCs. It is possible, perhaps likely that nature has discovered metal-mediated reactivities that are accessible to many different systems where product outcomes diverge in response to small perturbations in enzyme active sites. Understanding the detailed mechanisms of these metal-mediated processing reactions is important in the quest to expand the utility of these molecules as drug targets, and to develop synthetic biological protocols for their production.

Abbreviations

RiPP	Ribosomally synthesized and post translational modified peptide synthesis
PAM	Peptidylglycine alpha amidating monooxygenase
PHM	Peptidylglycine alpha hydroxylating monooxygenase
PHMcc	PHM catalytic core
BURP	BNM2, USP, RD22, and PG1beta
BpC	Burpitide cyclase
SAM	*S*-adenosyl methionine
RS	Radical SAM enzyme
DBM	Dopamine beta monooxygenase
Ac-YVG	Acetyl-tyr-val-gly
XAS	X-ray absorption
EXAFS	Extended X-ray absorption fine structure
EPR	Electron paramagnetic resonance
RFQ	Rapid freeze quench
FTIR	Fourier transform infra red
KIE	Kinetic isotope effect
HAA	Hydrogen atom abstraction
QM/MM	Quantum mechanics/molecular mechanics
DFT	Density functional theory
ET	Electron transfer
PCET	Proton coupled electron transfer
RMSD	Root mean square deviation
MV	Mixed valence
IVCT	Intervalence charge transfer

Data availability

No primary research results, software or code have been included, and no new data were generated or analyzed as part of this review.

Conflicts of interest

There are no conflicts to declare.

Acknowledgements

The work was funded by a grant to NJB from the National Institutes of Health NIGMS R35 GM136239. The work described herein is that of many talented post-doctoral fellows and graduate students over the years who have made important contributions to Blackburn lab publications. Recent studies form our lab on characterizing the binuclear state of PHM have been particularly aided by colleagues Dr Vahe Bandarian, Dr Renee Arias, Dr Katherine Rush Dr Karsten Eastman and Dr Evan Welch. XAS data were measured at the Stanford Synchrotron Radiation Lightsource and we are particularly grateful for the help and expertise of the beam line staff.

References

1 D. N. Chigumba, L. S. Mydy, F. de Waal, W. Li, K. Shafiq, J. W. Wotring, O. G. Mohamed, T. Mladenovic, A. Tripathi, J. Z. Sexton, S. Kautsar, M. H. Medema and R. D. Kersten, *Nat. Chem. Biol.*, 2022, **18**, 18–28.
2 G. A. Hudson and D. A. Mitchell, *Curr. Opin. Microbiol.*, 2018, **45**, 61–69.
3 D. J. Merkler, A. J. Hawley, B. A. Eipper and R. E. Mains, *Br. J. Pharmacol.*, 2022, **179**, 3306–3324.
4 M. Montalban-Lopez, T. A. Scott, S. Ramesh, I. R. Rahman, A. J. van Heel, J. H. Viel, V. Bandarian, E. Dittmann, O. Genilloud, Y. Goto, M. J. Grande Burgos, C. Hill, S. Kim, J. Koehnke, J. A. Latham, A. J. Link, B. Martinez, S. K. Nair, Y. Nicolet, S. Rebuffat, H. G. Sahl, D. Sareen, E. W. Schmidt, L. Schmitt, K. Severinov, R. D. Sussmuth, A. W. Truman, H. Wang, J. K. Weng, G. P. van Wezel, Q. Zhang, J. Zhong, J. Piel, D. A. Mitchell, O. P. Kuipers and W. A. van der Donk, *Nat. Prod. Rep.*, 2021, **38**, 130–239.
5 S. P. Brothers and C. Wahlestedt, *EMBO Mol. Med.*, 2010, **2**, 429–439.
6 B. Jones, *Br. J. Pharmacol.*, 2022, **179**, 492–510.
7 L. Zhang, C. Wang, K. Chen, W. Zhong, Y. Xu and I. Molnar, *Nat. Prod. Rep.*, 2023, **40**, 62–88.
8 K. W. Rush, K. A. S. Eastman, W. M. Kincannon, N. J. Blackburn and V. Bandarian, *J. Am. Chem. Soc.*, 2023, **145**, 10167–10177.
9 E. F. Welch, K. W. Rush, R. J. Arias and N. J. Blackburn, *J. Inorg. Biochem.*, 2022, **231**, 111780.
10 L. S. Mydy, J. Hungerford, D. N. Chigumba, J. R. Konwerski, S. C. Jantzi, D. Wang, J. L. Smith and R. D. Kersten, *Nat. Chem. Biol.*, 2024, **20**, 530–540.
11 J. R. Chekan, L. S. Mydy, M. A. Pasquale and R. D. Kersten, *Nat. Prod. Rep.*, 2024, **41**, 1020–1059.
12 C. Y. Chiang, M. Ohashi and Y. Tang, *J. Am. Chem. Soc.*, 2025, **147**, 8113–8117.
13 J. P. Klinman, *J. Biol. Chem.*, 2006, **281**, 3013–3016.
14 J. P. Klinman, *Chem. Rev.*, 1996, **1996**, 2541–2561.

15 T. V. Vendelboe, P. Harris, Y. Zhao, T. S. Walter, K. Harlos, K. El Omari and H. E. Christensen, *Sci. Adv.*, 2016, **2**, E1500980.
16 C. R. Hess, J. P. Klinman and N. J. Blackburn, *J. Biol. Inorg. Chem.*, 2010, **15**, 1195–1207.
17 C. W. Koo and A. C. Rosenzweig, *Chem. Soc. Rev.*, 2021, **50**, 3424–3436.
18 F. J. Tucci, R. J. Jodts, B. M. Hoffman and A. C. Rosenzweig, *Nat. Catal.*, 2023, **6**, 1194–1204.
19 F. J. Tucci and A. C. Rosenzweig, *Chem. Rev.*, 2024, **124**, 1288–1320.
20 J. O. Ipsen, M. Hallas-Moller, S. Brander, L. Lo Leggio and K. S. Johansen, *Biochem. Soc. Trans.*, 2021, **49**, 531–540.
21 G. C. Schroder, W. B. O'Dell, S. P. Webb, P. K. Agarwal and F. Meilleur, *Chem. Sci.*, 2022, **13**, 13303–13320.
22 S. T. Prigge, A. S. Kolhekar, B. A. Eipper, R. E. Mains and L. M. Amzel, *Science*, 1997, **278**, 1300–1305.
23 S. T. Prigge, A. S. Kolhekar, B. A. Eipper, R. E. Mains and L. M. Amzel, *Nat. Struct. Biol.*, 1999, **6**, 976–983.
24 S. T. Prigge, B. A. Eipper, R. E. Mains and L. M. Amzel, *Science*, 2004, **304**, 864–867.
25 K. Rudzka, D. M. Moreno, B. Eipper, R. Mains, D. A. Estrin and L. M. Amzel, *J. Biol. Inorg. Chem.*, 2013, **18**, 223–232.
26 E. E. Chufan, S. T. Prigge, X. Siebert, B. A. Eipper, R. E. Mains and L. M. Amzel, *J. Am. Chem. Soc.*, 2010, **132**, 15565–15572.
27 X. Siebert, B. A. Eipper, R. E. Mains, S. T. Prigge, N. J. Blackburn and L. M. Amzel, *Biophys. J.*, 2005, **89**, 3312–3319.
28 P. Chen, J. Bell, B. A. Eipper and E. I. Solomon, *Biochemistry*, 2004, **43**, 5735–5747.
29 B. A. Eipper, A. S. W. Quon, R. E. Mains, J. S. Boswell and N. J. Blackburn, *Biochemistry*, 1995, **34**, 2857–2865.
30 E. F. Welch, K. W. Rush, R. J. Arias and N. J. Blackburn, *Biochemistry*, 2022, **61**, 665–677.
31 J. S. Boswell, B. J. Reedy, R. Kulathila, D. J. Merkler and N. J. Blackburn, *Biochemistry*, 1996, **35**, 12241–12250.
32 J. C. Freeman, J. J. Villafranca and D. J. Merkler, *J. Am. Chem. Soc.*, 1993, **115**, 4923–4924.
33 N. J. Blackburn, M. Concannon, S. Khosrow Shahiyan, F. E. Mabbs and D. Collison, *Biochemistry*, 1988, **27**, 6001–6008.
34 N. J. Blackburn, F. C. Rhames, M. Ralle and S. Jaron, *J. Biol. Inorg. Chem.*, 2000, **5**, 341–353.
35 A. T. Bauman, B. A. Broers, C. D. Kline and N. J. Blackburn, *Biochemistry*, 2011, **50**, 10819–10828.
36 C. D. Kline and N. J. Blackburn, *Biochemistry*, 2016, **55**, 6652–6661.
37 S. Chauhan, C. D. Kline, M. Mayfield and N. J. Blackburn, *Biochemistry*, 2014, **53**, 1069–1080.
38 C. D. Kline, M. Mayfield and N. J. Blackburn, *Biochemistry*, 2013, **52**, 2586–2596.
39 R. A. Himes, G. Y. Park, G. S. Siluvai, N. J. Blackburn and K. D. Karlin, *Angew. Chem., Int. Ed.*, 2008, **47**, 9084–9087.
40 R. A. Himes, Y. G. Park, A. N. Barry, N. J. Blackburn and K. D. Karlin, *J. Am. Chem. Soc.*, 2007, **129**, 5352–5353.
41 I. J. Pickering, G. N. George, C. T. Dameron, B. Kurz, D. R. Winge and I. G. Dance, *J. Am. Chem. Soc.*, 1993, **115**, 9498–9505.
42 N. R. McIntyre, E. W. Lowe, Jr., J. L. Belof, M. Ivkovic, J. Shafer, B. Space and D. J. Merkler, *J. Am. Chem. Soc.*, 2010, **132**, 16393–16402.
43 W. A. Francisco, D. J. Merkler, N. J. Blackburn and J. P. Klinman, *Biochemistry*, 1998, **37**, 8244–8252.
44 W. A. Francisco, M. J. Knapp, N. J. Blackburn and J. P. Klinman, *J. Am. Chem. Soc.*, 2002, **124**, 8194–8195.
45 J. P. Evans, K. Ahn and J. P. Klinman, *J. Biol. Chem.*, 2003, **278**, 49691–49698.
46 J. P. Klinman, *Biochim. Biophys. Acta.*, 2006, **1757**, 981–987.
47 J. P. Evans, N. J. Blackburn and J. P. Klinman, *Biochemistry*, 2006, **45**, 15419–15429.
48 A. Crespo, M. A. Marti, A. E. Roitberg, L. M. Amzel and D. A. Estrin, *J. Am. Chem. Soc.*, 2006, **128**, 12817–12828.
49 P. Wu, F. Fan, J. Song, W. Peng, J. Liu, C. Li, Z. Cao and B. Wang, *J. Am. Chem. Soc.*, 2019, **141**, 19776–19789.
50 P. Chen and E. I. Solomon, *J. Am. Chem. Soc.*, 2004, **126**, 4991–5000.
51 P. Chen and E. I. Solomon, *Proc. Natl. Acad. Sci. U. S. A.*, 2004, **101**, 13105–13110.
52 R. E. Cowley, L. Tian and E. I. Solomon, *Proc. Natl. Acad. Sci. U. S. A.*, 2016, **113**, 12035–12040.
53 J. W. Ginsbach, R. L. Peterson, R. E. Cowley, K. D. Karlin and E. I. Solomon, *Inorg. Chem.*, 2013, **52**, 12872–12874.
54 S. Debnath, S. Laxmi, O. McCubbin Stepanic, S. Y. Quek, M. van Gastel, S. DeBeer, T. Kramer and J. England, *J. Am. Chem. Soc.*, 2024, **146**, 23704–23716.
55 M. Pasquali and C. Floriani, in *Copper Coordination Chemistry, Biochemical and Inorganic Perspectives*, ed K. D. Karlin and J. Zubieta, Adenine Press, New York, 1984, pp. 311–330.
56 H. C. Fry, H. R. Lucas, A. A. Sarjeant, K. D. Karlin and G. J. Meyer, *Inorg. Chem.*, 2008, **47**, 241–256.
57 I. Sanyal, K. D. Karlin, R. W. Strange and N. J. Blackburn, *J. Am. Chem. Soc.*, 1993, **115**, 11259–11270.
58 N. J. Blackburn, T. M. Pettingill, K. S. Seagraves and R. T. Shigeta, *J. Biol. Chem.*, 1990, **265**, 15383–15386.
59 T. M. Pettingill, R. W. Strange and N. J. Blackburn, *J. Biol. Chem.*, 1991, **266**, 16996–17003.
60 S. Jaron and N. J. Blackburn, *Biochemistry*, 1999, **38**, 15086–15096.
61 R. J. Arias, E. F. Welch and N. J. Blackburn, *Protein Sci.*, 2023, **32**, e4615.
62 P. Chen, D. E. Root, C. Campochiaro, K. Fujisawa and E. I. Solomon, *J. Am. Chem. Soc.*, 2003, **125**, 466–474.
63 R. L. Peterson, J. W. Ginsbach, R. E. Cowley, M. F. Qayyum, R. A. Himes, M. A. Siegler, C. D. Moore, B. Hedman, K. O. Hodgson, S. Fukuzumi, E. I. Solomon and K. D. Karlin, *J. Am. Chem. Soc.*, 2013, **135**, 16454–16467.
64 J. S. Woertink, L. Tian, D. Maiti, H. R. Lucas, R. A. Himes, K. D. Karlin, F. Neese, C. Wurtele, M. C. Holthausen, E. Bill, J. Sundermeyer, S. Schindler and E. I. Solomon, *Inorg. Chem.*, 2010, **49**, 9450–9459.

65 R. L. Peterson, R. A. Himes, H. Kotani, T. Suenobu, L. Tian, M. A. Siegler, E. I. Solomon, S. Fukuzumi and K. D. Karlin, *J. Am. Chem. Soc.*, 2011, **133**, 1702–1705.
66 T. Tano, Y. Okubo, A. Kunishita, M. Kubo, H. Sugimoto, N. Fujieda, T. Ogura and S. Itoh, *Inorg. Chem.*, 2013, **52**, 10431–10437.
67 A. Kunishita, M. Z. Ertem, Y. Okubo, T. Tano, H. Sugimoto, K. Ohkubo, N. Fujieda, S. Fukuzumi, C. J. Cramer and S. Itoh, *Inorg. Chem.*, 2012, **51**, 9465–9480.
68 A. Kunishita, M. Kubo, H. Sugimoto, T. Ogura, K. Sato, T. Takui and S. Itoh, *J. Am. Chem. Soc.*, 2009, **131**, 2788–2789.
69 S. Kim, J. Y. Lee, R. E. Cowley, J. W. Ginsbach, M. A. Siegler, E. I. Solomon and K. D. Karlin, *J. Am. Chem. Soc.*, 2015, **137**, 2796–2799.
70 B. N. Sanchez-Eguia, M. Flores-Alamo, M. Orio and I. Castillo, *Chem. Commun.*, 2015, **51**, 11134–11137.
71 K. B. Alwan, E. F. Welch, R. J. Arias, B. F. Gambill and N. J. Blackburn, *Biochemistry*, 2019, **58**, 3097–3108.
72 K. B. Alwan, E. F. Welch and N. J. Blackburn, *Biochemistry*, 2019, **58**, 4436–4446.
73 K. W. Rush, K. B. Alwan, A. T. Conner, E. F. Welch and N. J. Blackburn, *Inorg. Chem.*, 2024, **63**, 21519–21530.
74 R. J. Arias, E. F. Welch and N. J. Blackburn, *Protein Sci.*, 2023, **32**, e4615.
75 S. Jaron, R. E. Mains, B. A. Eipper and N. J. Blackburn, *Biochemistry*, 2002, **41**, 13274–13282.
76 G. Y. Park, J. Y. Lee, R. A. Himes, G. S. Thomas, N. J. Blackburn and K. D. Karlin, *J. Am. Chem. Soc.*, 2014, **136**, 12532–12535.
77 L. Y. Fager and J. O. Alben, *Biochemistry*, 1972, **11**, 4786–4792.
78 R. B. Dyer, O. Einarsdottir, P. M. Killough, G. J. J. Lopez and W. H. Woodruff, *J. Am. Chem. Soc.*, 1989, **111**, 7657–7659.
79 I. Sanyal, K. D. Karlin, R. W. Strange and N. J. Blackburn, *J. Am. Chem. Soc.*, 1993, **115**, 11259–11270.
80 S. Kealy, A. J. P. White, A. D. Gee and N. J. Long, *Eur. J. Inorg. Chem.*, 2014, 1896–1905.
81 Y. Lee, G. Y. Park, H. R. Lucas, P. L. Vajda, K. Kamaraj, M. A. Vance, A. E. Milligan, J. S. Woertink, M. A. Siegler, A. A. Narducci Sarjeant, L. N. Zakharov, A. L. Rheingold, E. I. Solomon and K. D. Karlin, *Inorg. Chem.*, 2009, **48**, 11297–11309.
82 G. B. Ray, X.-Y. Li, J. A. Ibers, J. L. Sessler and T. G. Spiro, *J. Am. Chem. Soc.*, 1994, **116**, 162–176.
83 O. Einarsdottir, P. M. Killough, J. A. Fee and W. H. Woodruff, *J. Biol. Chem.*, 1989, **264**, 2405–2408.
84 C. A. Ramsden and P. A. Riley, *Bioorg. Med. Chem.*, 2014, **22**, 2388–2395.
85 T. Klabunde, C. Eicken, J. C. Sacchettini and B. Krebs, *Nat. Struct. Biol.*, 1998, **5**, 1084–1090.
86 S. M. Miller and J. P. Klinman, *Biochemistry*, 1985, **24**, 2114–2127.
87 S. Maheshwari, C. Shimokawa, K. Rudzka, C. D. Kline, B. A. Eipper, R. E. Mains, S. B. Gabelli, N. Blackburn and L. M. Amzel, *Commun. Biol.*, 2018, **1**, 74.
88 M. D. Erion, J. Tan, M. Wong and A. Y. Jeng, *J. Med. Chem.*, 1994, **37**, 4430–4437.
89 K. W. Rush, K. A. S. Eastman, E. F. Welch, V. Bandarian and N. J. Blackburn, *J. Am. Chem. Soc.*, 2024, **146**, 5074–5080.
90 D. R. Gamelin, D. W. Randall, M. T. Hay, R. P. Houser, T. C. Mulder, G. W. Canters, S. de Vries, W. B. Tolman, Y. Lu and E. I. Solomon, *J. Am. Chem. Soc.*, 1998, **120**, 5246–5263.
91 R. P. Houser, V. G. J. Young and W. B. Tolman, *J. Am. Chem. Soc.*, 1996, **118**, 2101–2102.
92 K. N. Chacon and N. J. Blackburn, *J. Am. Chem. Soc.*, 2012, **134**, 16401–16412.
93 S. Chakraborty, M. J. Polen, K. N. Chacon, T. D. Wilson, Y. Yu, J. Reed, M. J. Nilges, N. J. Blackburn and Y. Lu, *Biochemistry*, 2015, **54**, 6071–6081.
94 P. A. Williams, N. J. Blackburn, D. Sanders, H. Bellamy, E. A. Stura, J. A. Fee and D. E. McRee, *Nat. Struct. Biol.*, 1999, **6**, 509–516.
95 N. J. Blackburn, S. de Vries, M. E. Barr, R. P. Houser, W. B. Tolman, D. Sanders and J. A. Fee, *J. Am. Chem. Soc.*, 1997, **119**, 6135–6143.
96 K. R. Williams, D. R. Gamelin, L. B. Lacroix, R. P. Houser, W. B. Tolman, M. C. Mulder, S. de Vries, B. Hedman, K. O. Hodgson and E. I. Solomon, *J. Am. Chem. Soc.*, 1997, **119**, 613–614.
97 T. Haltia, K. Brown, M. Tegoni, C. Cambillau, M. Saraste, K. Mattila and K. Djinovic-Carugo, *Biochem. J.*, 2003, **369**, 77–88.
98 P. M. H. Kroneck, *J. Biol. Inorg. Chem.*, 2018, **23**, 27–39.
99 M. N. Morgada, D. H. Murgida and A. J. Vila, *Met. Ions Life Sci.*, 2020, **20**, DOI: **10.1515/9783110589757-010**.
100 M. T. Hay, M. C. Ang, D. R. Gamelin, E. I. Solomon, W. E. Antholine, M. Ralle, N. J. Blackburn, P. D. Massey, X. Wang, A. H. Kwon and Y. Lu, *Inorg. Chem.*, 1998, **37**, 191–198.
101 H. Robinson, M. C. Ang, Y.-G. Gao, M. T. Hay, Y. Lu and A. H.-J. Wang, *Biochemistry*, 1999, **38**, 5677–5683.
102 M. O. Ross, O. S. Fisher, M. N. Morgada, M. D. Krzyaniak, M. R. Wasielewski, A. J. Vila, B. M. Hoffman and A. C. Rosenzweig, *J. Am. Chem. Soc.*, 2019, **141**, 4678–4686.
103 T. D. Westmoreland, D. E. Wilcox, M. J. Baldwin, W. B. Mims and E. I. Solomon, *J. Am. Chem. Soc.*, 1989, **111**, 6106–6123.
104 B. Hazes, K. A. Magnus, C. Bonaventura, J. Bonaventura, Z. Dauter, K. H. Kalk and W. G. Hol, *Prot. Sci.*, 1993, **2**, 597–619.
105 K. A. Magnus, B. Hazes, H. Ton-That, C. Bonaventura, J. Bonaventura and W. G. J. Hol, *Proteins: Struct., Funct., Genet.*, 1994, **19**, 302–309.
106 E. F. Welch, K. W. Rush, K. A. S. Eastman, V. Bandarian and N. J. Blackburn, *Dalton Trans.*, 2025, **54**, 4941–4955.
107 M. M. Kimani, J. L. Brumaghim and D. VanDerveer, *Inorg. Chem.*, 2010, **49**, 9200–9211.
108 B. N. Sánchez-Eguía, H. Hernández-Toledo, S. Lidin, M. Flores-Alamo, E. Nordlander, S. Bertaina, M. Orio and I. Castillo, *ChemCatChem*, 2025, **17**, e202401330.
109 Y. Chen, J. Wang, G. Li, Y. Yang and W. Ding, *Front. Chem.*, 2021, **9**, 595991.

110 J. A. Latham, I. Barr and J. P. Klinman, *J. Biol. Chem.*, 2017, **292**, 16397–16405.
111 N. A. Bruender, J. Wilcoxen, R. D. Britt and V. Bandarian, *Biochemistry*, 2016, **55**, 2122–2134.
112 T. L. Grove, P. M. Himes, S. Hwang, H. Yumerefendi, J. B. Bonanno, B. Kuhlman, S. C. Almo and A. A. Bowers, *J. Am. Chem. Soc.*, 2017, **139**, 11734–11744.
113 A. T. Bauman, E. T. Yukl, K. Alkevich, A. L. McCormack and N. J. Blackburn, *J. Biol. Chem.*, 2006, **281**, 4190–4198.
114 M. Bhadra, W. J. Transue, H. Lim, R. E. Cowley, J. Y. C. Lee, M. A. Siegler, P. Josephs, G. Henkel, M. Lerch, S. Schindler, A. Neuba, K. O. Hodgson, B. Hedman, E. I. Solomon and K. D. Karlin, *J. Am. Chem. Soc.*, 2021, **143**, 3707–3713.